Theoretical and practical investigations concerning the design of a HOM broadband absorber for TESLA

A. Jöstingmeier*, M. Dohlus*, M. Wendt* and C. Cramer†

*Deutsches Elektronen-Synchrotron DESY
Gruppe Beschleunigerphysik
Notkestr. 85, D-22603 Hamburg, Germany

†Wilhelms-Universtät Münster
Institut für Physikalische Chemie
Schloßplatz 4/7, D-48149 Münster, Germany

Abstract

In this contribution the design of a HOM (higher order mode) broadband absorber for TESLA is theoretically investigated using a distortion analysis based on the results of a modal expansion of the cavity field. The GSM (generalized scattering matrix) method is applied for the computation of more than 1000 TM monopole modes of a TESLA 9cell cavity to which an absorber cell is connected. In order to measure the absorption properties of a material a planar model is introduced for which a so-called absorber efficiency is defined. The electromagnetic properties of two absorbers, namely glassy $0.5AgI*0.5AgPO_3$ and MACOR (Corning MACOR™ Machinable Glass Ceramic is a product of Corning Glas Works, Corning, NY), are discussed. The effects of these absorbers for a TESLA 9cell cavity are analyzed. An experimental setup is described which is used to validate the theoretical results by measurements. For this experiment a method for the calculation of the internal quality factors of a structure from its frequency dependent input reflection is developed. The results of the measurements for a TESLA 9cell cavity with and without absorber are presented and compared with the theoretical predictions.

Contents

I Introduction

In the FEL (free electron laser) mode of TESLA very short and intense bunches of particles are accelerated [1], [2]. Keeping in mind that for the single bunch energy loss W_{loss} the well-known relation

$$W_{loss} \propto q^2 \int_{\omega=0}^{\infty} \underbrace{\mathrm{Re}\{Z(\omega)\}}_{>0} |\lambda(\omega)|^2 \, d\omega \tag{1}$$

holds, where q, $Z(\omega)$ and $\lambda(\omega)$ are the bunch charge, the beam impedance and the bunch spectrum, respectively, it follows that W_{loss} becomes large for such bunches. Fig. 1 presents $\lambda(f)$

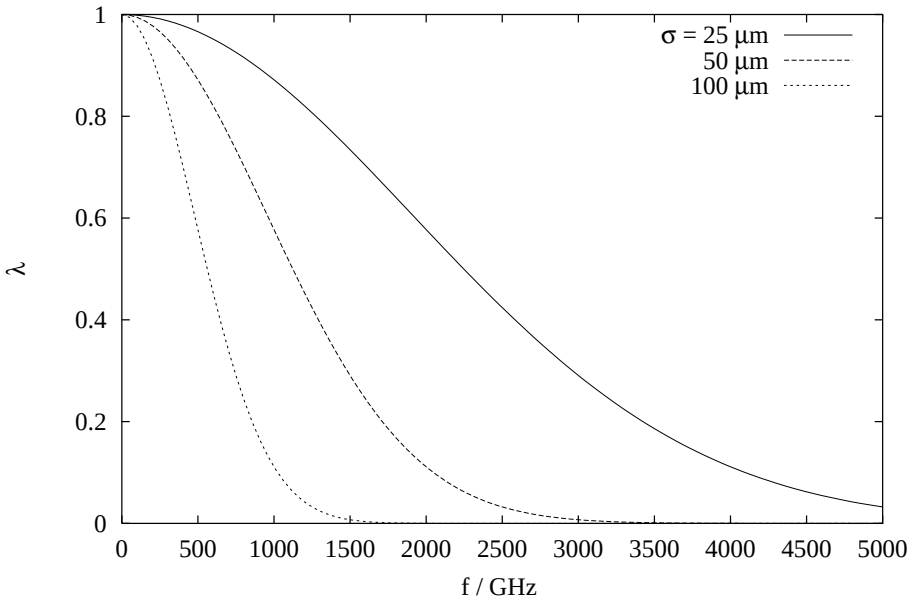

Figure 1: Bunch spectra $\lambda(f)$ for various bunches.

for various bunches. The curves which are shown in this figure illustrate that the spectrum of a typical FEL bunch with $\sigma = 25\,\mu$m extends up to frequencies of some THz.

Table 1 gives the dissipated power due to single bunch energy loss for the FEL mode of

$\sigma = 50\,\mu$m	$f > 20\,$GHz	$f > 800\,$GHz
single cavity model	27.6 W	3.6 W
periodic model	3.8 W	0.1 W

$\sigma = 25\,\mu$m	$f > 20\,$GHz	$f > 800\,$GHz
single cavity model	41.2 W	14.4 W
periodic model	4.1 W	0.3 W

Table 1: Single bunch losses in a TESLA module for $50\,\mu$m and $25\,\mu$m long bunches. Parameters: Bunch charge = 1 nC and $5 \cdot 11315$ bunches/s.

TESLA. The numbers resulting from a single cavity and a periodic model are presented in

this table for 50 μm and 25 μm long bunches. The single cavity model is based on a diffraction model which makes use of the assumptions that the circular cavity aperture may be replaced by a straight edge and that the electromagnetic field in the beampipe is similar to that of a plane wave near the beampipe shielding. The contributions of the individual cells are assumed to be independent and thus simply add up.

On the other hand, if we consider a string of accelerator cells we have to take into account that the already generated HOM fields which travel with the bunch are also influenced by the upstream cells. This effect is included in the so-called periodic model which was investigated in [3]. It is based on a time domain computation of the wakefields for up to two TESLA modules. It is known that the transition between the regimes where the single cavity model holds and that where the periodic model is valid takes place after a large number of cells if we consider short bunches. It was found out in [3] that even after two modules the simulated wakefields are not stable for a 50 μm bunch. However it seems to be well-justified to assume that the numbers corresponding to the periodic model are the relevant ones if we look at the entire accelerator. A detailed comparison of both models is given in [4]. It is interesting to note that the single cavity model always yields a higher power loss than the periodic model.

About 800 W of wall plug power are required in a typical refrigerator per Watt dissipated at 2 K [5]. In the current design proposal of TESLA two HOM couplers are foreseen per module. Let us assume that these couplers work perfectly up to a frequency of 20 GHz, then we expect approximately 4.1 W of dissipated power per module for a 25 μm long bunch. This means that about 3.3 kW of cooling power per module are necessary only due to the HOM losses. This number underlines that it is really desirable to absorb as much as possible of these losses at a higher temperature level than 2 K, e.g. at 70 K, where the refrigerator efficiency is much better. Table 2 gives the power consumption per Watt heat load and the cryogenic efficiency of a

Temperature	2 K	4 K	70 K
Wall plug power/ Watt heat load	800 W	250 W	25 W
Cryogenic efficiency	0.125%	0.4%	4%

Table 2: Power consumption per Watt heat load and cryogenic efficiency of a typical refrigerator.

typical refrigerator at 2 K, 4 K and 70 K.

Spectral components of the cavity fields above 750 GHz can crack the Cooper pairs in the niobium which leads to a considerable increase of the real part of the surface impedance of the wall material. The surface resistivity of niobium at 2 K increases roughly by a factor of 10000 between 600 GHz and 1 THz. Most of the wakefields with $f > 800$ GHz are thus already absorbed within the cavity where they are generated. Consequently, these losses cannot be accesssed efficiently by a HOM absorber which has to be outside the cavities.

The power loss between 20 GHz and 800 GHz amounts to about 3.8 W in the periodic model. Using a HOM absorber it can be partly avoided that these losses occur at the 2 K level. If we assume that the absorber does not work perfectly and only 90% of the accessible HOM losses can be extracted, the wall plug power for the cooling can still be reduced by more than 2.7 kW per module.

A HOM absorber which is sketched in Fig. 2 was already proposed in [5] and [6]. This absorber consists of an array of outward directed rectangular waveguides surrounding the beampipe. The extraction of the high frequency wakefields by such an array has been investi-

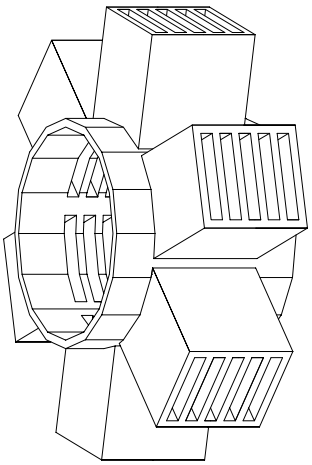

Figure 2: Schematic drawing of a waveguide HOM absorber.

gated in detail in [7]–[9]. Note that Fig. 2 just shows a schematic drawing of the HOM absorber; the actual absorber consists of an array of about 140×250 waveguides in the azimuthal and the axial direction, respectively. It is obvious that the manufacturing of such a structure is extremely difficult and costly even if etching techniques are applied [5]. Furthermore the problem of cleaning the waveguide array before it is installed in the TESLA vacuum system has yet not been solved.

Therefore four new absorber structures which are much easier to fabricate and better suited for operation under vacuum conditions with respect to cleaning and pumping were suggested in [5]. The proposed structures are shown in Figs. 3–6. In each of these configurations the actual absorbing structure is accomodated in a shielding which is similar to a single cell of the TESLA accelerating structure. It was demonstrated that the solid and the metallized laminated absorber have good absorption properties. The simulation results had shown that the efficiency of the absorbers is not significantly decreased if we hide the actual absorbing structure behind the iris of the shielding cavity. The short range wake of such a hidden structure is equal to that of a single TESLA accelerating cell for short bunches; and it is still tolerable for an intermediate bunch length.

Concerning manufacturing and installation we clearly prefer the solid absorber because it basically consists of a pipe of absorber material which is accomodated in a shielding cavity. Hence the absorption properties of such a structure in a TESLA cavity is investigated in detail in this contribution which is organized as follows:

Paragraph II is dedicated to the field theoretical analysis of a TESLA accelerating cavity which is connected to an empty absorber cell. The GSM method is employed for the numerical investigation of this structure. The spectral density of the modes is an important input parameter for the application of the GSM method. In paragraph IIa) this quantity is estimated for TM monopole modes in a cylindrical cavity; and the result is then generalized to such modes in rotationally symmetric cavities. In order to increase the numerical efficiency of the GSM method a staircase approximation of the actual structure is used. The complete spectrum of TM monopole modes of this model is computed up to a frequency of 20 GHz in paragraph IIc). Besides the resonant frequency and the quality factor of each mode, the loss parameter is also determined. This quantity is required in paragraph IIIc) in order to calculate the excitation of a HOM by the beam. The numerical results are checked by comparing the computed quality factors with those corresponding to TM monopole modes of a cylindrical cavity which are

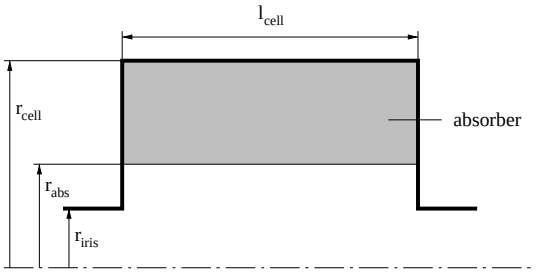

Figure 3: Solid absorber.

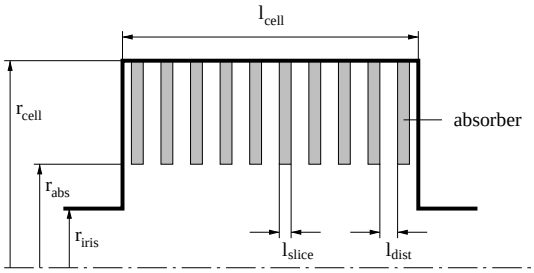

Figure 4: Laminated absorber.

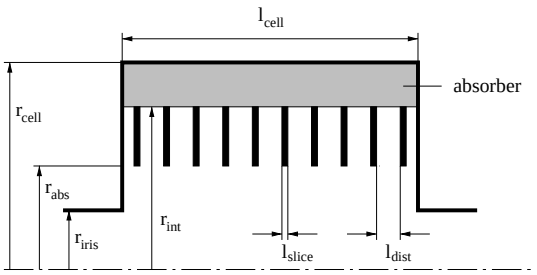

Figure 5: Combined absorber.

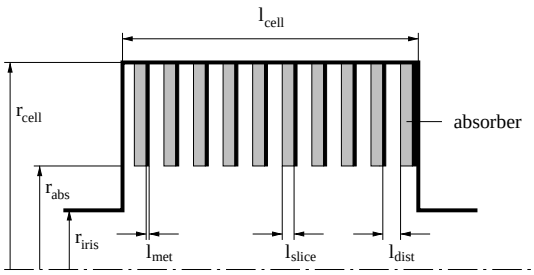

Figure 6: Metallized laminated absorber.

calculated in paragraph IIb).

The properties of two absorber materials, namely $0.5AgI*0.5AgPO_3$ and MACOR are discussed in paragraph III. The first material is a glas with high losses; whereas the latter one is a frequently used machinable ceramic. The transmission of a TEM wave through a lossy dielectric slab is studied in paragraph IIIa) in order to define a figure of merit for the performance of a material as absorber. This quantity is calculated for $0.5AgI*0.5AgPO_3$ and MACOR in paragraph IIIb).

The electromagnetic properties of $0.5AgI*0.5AgPO_3$ at a variety of temperatures were measured at the Universität Münster from almost DC up to the far infrared region. Several measurement techniques were combined in order to cover such a broad spectral range: Impedance measurements were carried out in the low frequency range, the scattering parameters of glas samples were determined in the intermediate frequency range (4 MHz ... 18 GHz coaxial line, 18 GHz ... 110 GHz rectangular waveguides from K to W band) and a Fourier spectrometer was used in the far infrared regime. Unfortunately $0.5AgI*0.5AgPO_3$ is not compatible with the ultra-vacuum conditions in an accelerator. This material serves us however as a reference absorber in order to demonstrate how much of the HOM losses can be extracted with a material that has high losses and a low permittivity.

MACOR is often used in the vacuum system of accelerators. The complex permittivity of this material at room temperature is well-known in a wide spectral range: In the literature one finds corresponding numbers up to a frequency of about 900 GHz. At the Universität Hamburg and at the Universität Münster measurements in the far infrared region starting from approximately 200 GHz up to 1.5 THz were carried out. On the other hand, we have only the FTIR-spectrometer measurements from Münster for MACOR at 88 K which is close to the temperature of liquid nitrogen. The measured permittivity spectrum at this temperature seems to be reliable for $f > 300$ GHz so that we cannot use these results for out modal analysis which

does not cover such high frequencies.

The effect of a $0.5AgI*0.5AgPO_3$ and a MACOR absorber on the distribution of the HOM losses in a TESLA 9cell cavity are investigated in paragraph IIIc) by using a distortion analysis. The quality factors which are computed in paragraph IIc) are valid for a structure which is completely made out of copper with an empty absorber cavity. The absorber and the fact that the wall material of the accelerating cavity is niobium at 2 K is taken into account by properly scaling the real part of the surface impedance of the individual parts of the structure. For the calculation of the individual excitation of each mode, which is an important quantity in order to compute the HOM losses properly, the above determined loss parameters are used.

In order to confirm the simulation results some measurements at a copper model of a TESLA 9cell cavity which is connected to an absorber cell are made. TM monopole modes are excited by a small coaxial antenna; and the input reflection is measured as a function of frequency using a vector network analyzer (VNA). The measurement setup is described in detail in paragraph IVa). In general many modes contribute significantly to the input reflection even at a resonance peak because the investigated structure is overmoded in the considered frequency range. Therefore a procedure is developed which can be used in order to calculate the internal quality factor of each mode from the measured reflection coefficient. In the following paragraph the results of some measurements with and without absorber material are discussed. The simulation results which are calculated for a copper structure are compared with the corresponding measurement results.

II Modal expansion

IIa) Number of modes

In order to estimate the number of TM monopole modes in a cylindrical cavity with resonant frequencies f_0 in the range $0 < f_0 < f$ we may recall the spatial dependence of the axial electric field E_z in such a structure:

$$E_z \propto \mathrm{J}_0(k_{\rho m}\rho)\cos(\beta_n z) \tag{2}$$

ρ and z denote the radial and the axial coordinate, repectively. $k_{\rho m}$ and β_n are the corresponding wavenumbers which read

$$k_{\rho m} = \frac{p_{0,m}}{a} \quad , \tag{3}$$

$$\beta_n = \frac{n\pi}{L} \quad , \tag{4}$$

where a and L are the radius and the length of the cylindrical cavity; and p_{0m} is the mth zero of the Bessel function J_0.

The axial wavenumbers β_n are equally spaced according to Eq. (4). This statement is also approximately valid in the radial direction if we consider eigenmodes with a large index m because

$$\lim_{m\to\infty} p_{0,m+1} - p_{0,m} = \pi \quad . \tag{5}$$

Nevertheless, even for $m = 1$ we have $p_{0,2} - p_{0,1} = 3.115$, which is already quite similar to π. Therefore we may assume that the wavenumbers of TM monopole modes in a cylindrical cavity are equally spaced in the radial and the axial direction.This is illustrated in Fig. 7. Let k denote

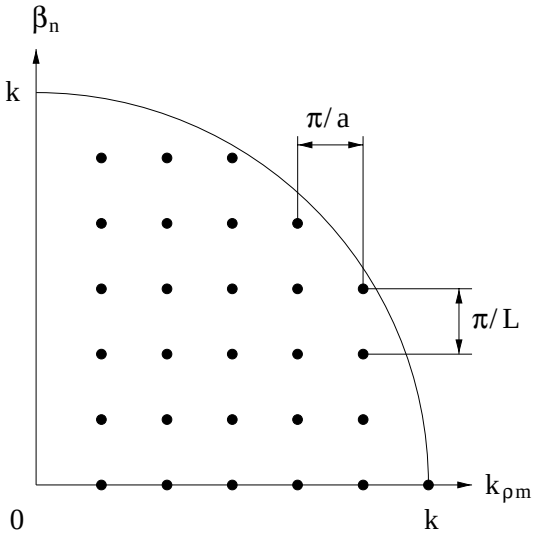

Figure 7: Approximate location of TM monopole modes of a cylindrical cavity in spectral domain.

the wavenumber that corresponds to the frequency f ($k = 2\pi f/c_0$), then all eigenmodes fulfill the condition

$$k_{\rho m}^2 + \beta_n^2 \leq k^2 \quad . \tag{6}$$

This means that all resonances are contained within the quarter circle which is shown in Fig. 7. In spectral domain this quarter circle covers an area

$$F = \frac{\pi k^2}{4} \quad . \tag{7}$$

On the other hand, the area A which corresponds to each mode is

$$A = \frac{\pi}{a}\frac{\pi}{L} \quad . \tag{8}$$

This means that the number of modes with wavenumbers between 0 and k is given by

$$N = \frac{F}{A} = \frac{\pi k^2}{4\frac{\pi}{a}\frac{\pi}{L}} \quad . \tag{9}$$

Let us rewrite the above equation in the following form:

$$\frac{N}{aL} = \pi \left(\frac{f}{c_0}\right)^2 \tag{10}$$

Eq. (10) clearly shows the well-known fact that the number of TM monople modes is proportional to f^2.

Note that the dimensions of the cavity appear only in the denominator on the left-hand-side of the above equation. The product aL is just the area of the cylindrical cavity in the ρz-plane. Let us extend our considerations to the more general case of TM monopole modes of rotationally symmetric cavities where the contour is given by a function $\rho(z)$. We intuitively substitute the term aL in Eq. (10) by $\int_{z=0}^{L} \rho(z)\, dz$ for such cavities. This integral equals $101279\,\mathrm{mm}^2$ for a TESLA 9cell cavity including beampipes and absorber cavity. For such a structure the frequency and the number of modes is related by

$$\frac{f}{\mathrm{GHz}} = 0.531\sqrt{N} \quad . \tag{11}$$

IIb) Quality factors of the TM monopole modes

Before we employ a numerical method in order to compute the resonant frequencies and quality factors of the TM monopole modes of the investigated structure it is instructive to see what is the fundamental behaviour of the quality factor as a function of frequency. For this study we use again the simple model of a cylindrical cavity.

According to [10], the power losses P^b_{loss} and P^c_{loss} at the bottom and the cylindrical surface of a cylindrical cavity divided by the total stored energy W^{tot} are given by the relations

$$\frac{P^b_{loss}}{W^{tot}} = \frac{2R_s}{\mu_0 \begin{cases} L & , \quad n = 0 \\ L/2 & , \quad n > 0 \end{cases}} \quad , \tag{12}$$

$$\frac{P^c_{loss}}{W^{tot}} = \frac{2R_s}{\mu_0 a} \quad . \tag{13}$$

R_s denotes the real part of the surface impedance of the wall material at the resonant frequency. This quantity reads

$$R_s = \frac{1}{\sigma \delta_s} \quad , \tag{14}$$

where σ and δ_s denote the conductivity of the material and the skin depth.

The skin depth is proportional to $1/\sqrt{\omega_0}$. Hence the total power loss P^{tot}_{loss} is proportional to $\sqrt{\omega_0}$:

$$P^{tot}_{loss} \propto \sqrt{\omega_0} \neq \mathrm{f}(k_{\rho m}) \tag{15}$$

It is interesting to note that P^{tot}_{loss} is neither a function of $k_{\rho m}$ nor of β_n; it is just proportional to the resonant frequency. Hence the quality factor is proportional to $\sqrt{\omega_0}$:

$$Q = \frac{\omega_0}{P^{tot}_{loss}/W^{tot}} \propto \sqrt{\omega_0} \tag{16}$$

This means that Q increases with increasing frequency which may be explained as follows: Although the total losses increase with increasing frequency according to Eq. (15), the energy loss per period, which is important for the calculation of the quality factor, decreases because the period length is inverse proportional to the resonant frequency.

Thus the damping time which is defined by the decay of an initial energy W^{tot}_0 of a mode according to

$$W^{tot}(t) = W^{tot}_0 e^{-t/T_d} \tag{17}$$

reads

$$T_d = \frac{Q}{\omega_0} \propto \frac{1}{\sqrt{\omega_0}} \quad . \tag{18}$$

Hence it is inverse proportional to $\sqrt{\omega_0}$.

IIc) Resonant frequencies, quality factors and loss parameters of a TESLA cavity

The GSM method has been proved accurate and numerically efficient for the investigation of a large variety of waveguide and cavity problems [11]–[13]. This method was also successfully applied in the field of linear accelerators [14]. In this paper it used to compute the resonant

frequencies and quality factors of a TESLA 9cell cavity including beampipes and the absorber cavity.

The GSM method is based on a staircase approximation of the actual structure. For the sake of simplicity let us approximate each iris of the TESLA cavity by a single step as it is shown in Fig. 8. The dimensions of the staircase model are chosen such that it covers the same

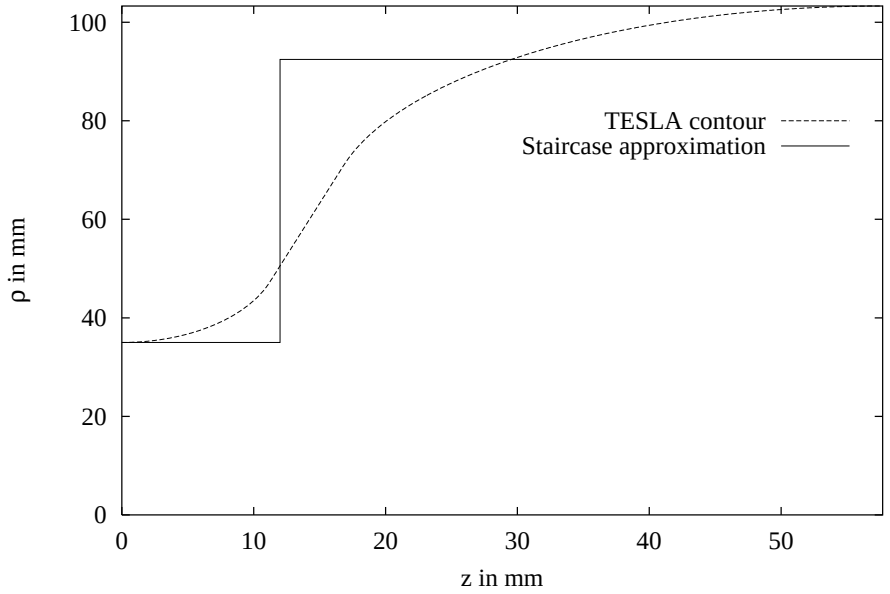

Figure 8: Staircase approximation of the contour of a TESLA cavity.

area in the ρz-plane as the actual structure.

Fig. 9 presents the contour of the model that we use for the numerical investigations. Each of the nine cells of the cavity is approximated by a box. Between the 9cell cavity and the absorber cavity a beampipe section with a length of 200 mm is assumed. The radial dimension of the absorber cavity is 10 mm larger than that of the beampipe so that enough space is available for the absorber material. In order to confine the electromagnetic energy inside the structure it is short-circuited at both ends.

Fig. 10 shows the resonant frequencies of the investigated structure as a function of the mode number. Each dot corresponds to one mode. The solid line represents our approximation according to Eq. (11). Fig. 10 underlines how well the actual number of modes is estimated by this simple relation. E.g., for 20 GHz, Eq. (11) predicts 1419 TM monopole modes whereas the actual number of modes is 1371.

Although much effort was spent in order to increase the numerical efficiency of the GSM method, its cpu-time requirement increases with ω^4. The analysis of strongly overmoded structures is therefore still quite time consuming even if a modern workstation is used. It took about one month of cpu-time on the solar cluster at DESY to calculate the modes which are presented in Fig. 10.

Fig. 11 shows the resonant frequencies of first 50 modes in more detail. The first three passbands of the TESLA cavity are well-separated. Each of them contains nine modes according to the number of cavity cells. On the other hand, the fourth and the fifth passband already overlap.

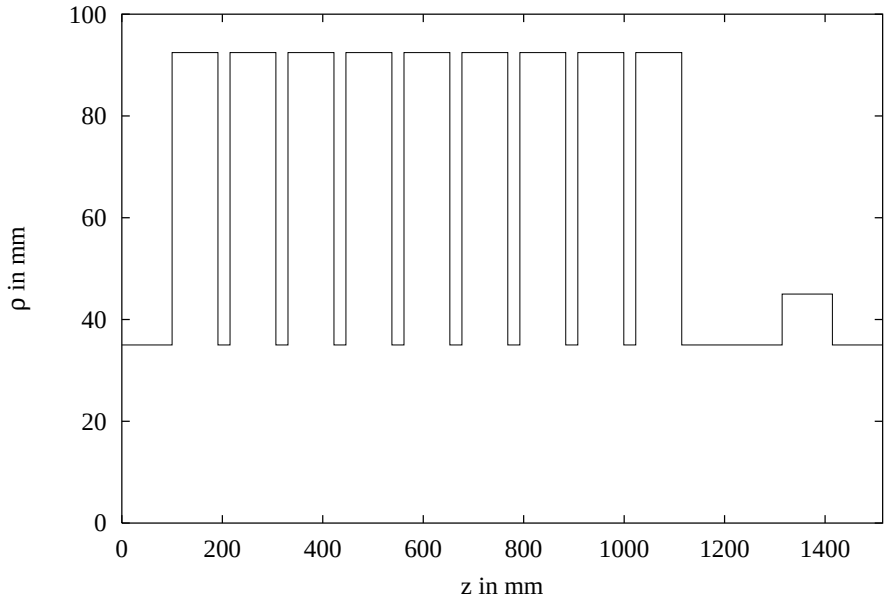

Figure 9: Contour of the investigated structure.

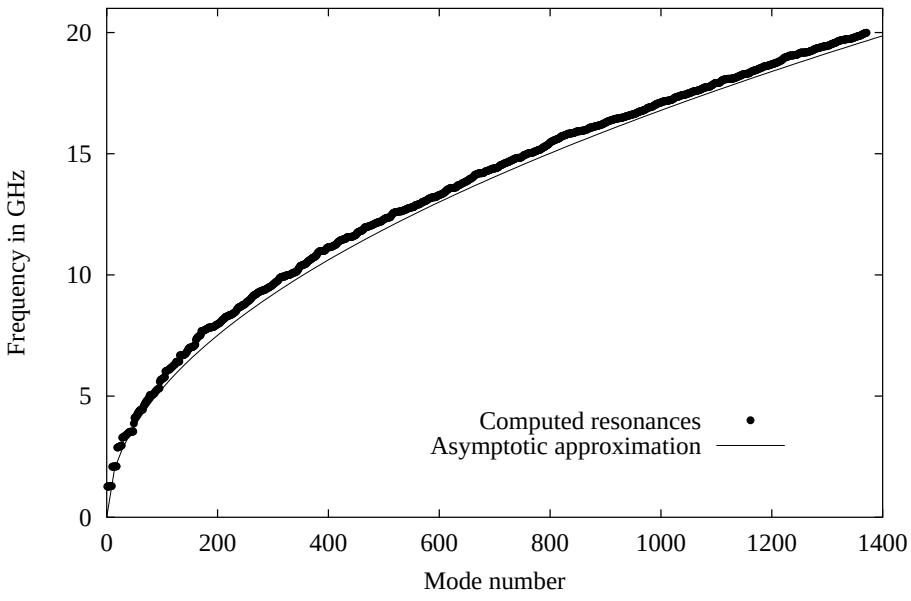

Figure 10: Resonant frequencies as a function of mode number for a TESLA 9cell cavity with HOM absorber.

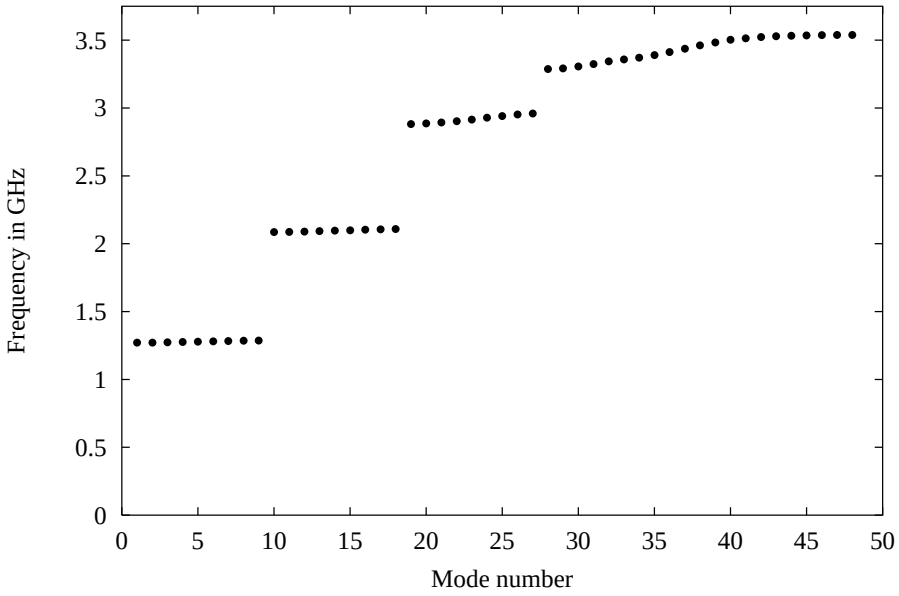

Figure 11: Resonant frequencies of the first 50 modes of the investigated structure.

The axial electric field E_z of the fundamental mode which has a resonant frequency of 1.2707 GHz is shown as a function of the axial coordinate in Fig. 12. E_z is in phase in all of

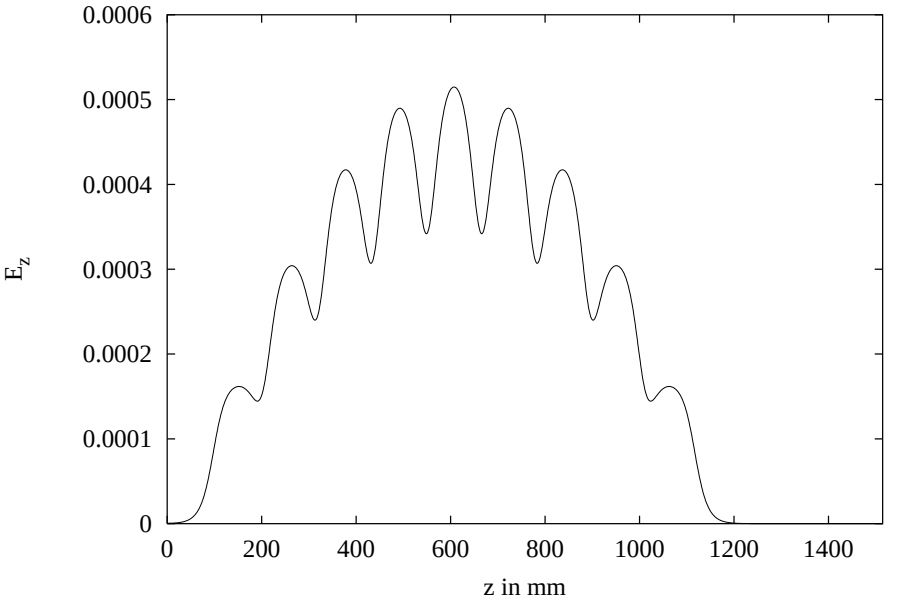

Figure 12: Axial electric field of the fundamental mode ($f_0 = 1.2707\,\mathrm{GHz}$) as a function of the axial coordinate.

the cells as expected for a zero-mode. Note that the field of the 9cell cavity cannot penetrate into the absorber cavity because the beampipe is far below cutoff in the frequency range of the first passband. Fig. 13 shows the axial electric field of the mode with the highest resonant frequency of the first passband which is used as accelerating mode in TESLA. This mode is

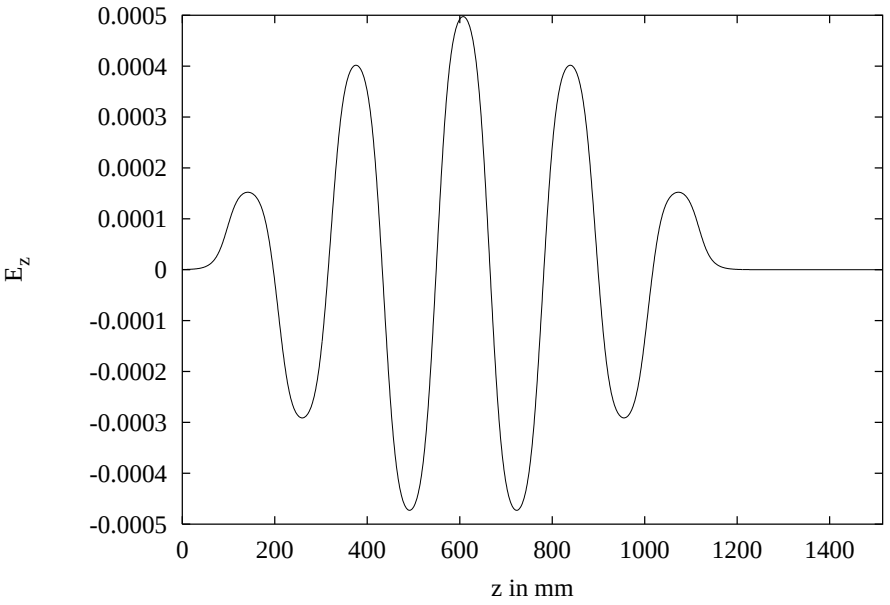

Figure 13: Axial electric field of the π-mode of the first passband ($f_0 = 1.2866\,\mathrm{GHz}$) as a function of the axial coordinate.

clearly a π-mode because the sign of E_z alternates from cell to cell.

For the computation of the quality factor of each cavity mode a perturbation theory is applied which was already used in the previous paragraph for the calculation of the Q of TM monopole modes in a cylindrical cavity. This theory is based on the assumption that the electromagnetic field of each mode is essentially the same as that of the corresponding lossless structure. The ohmic losses are taken into account by the real part of the surface impedance R_s which leads to Eqs. (12) and (13) for a cylindrical cavity. In general, the quality factor of a mode may be calculated using Eq. (16) with

$$P_{loss}^{tot} = \frac{1}{2} \oint_S R_s \, |\boldsymbol{H}|^2 \, dS \quad , \tag{19}$$

$$W^{tot} = \frac{\mu_0}{2} \int_V |\boldsymbol{H}|^2 \, dV \quad , \tag{20}$$

where $\boldsymbol{H}$, V and S denote the magnetic field of the resonant mode, the volume and the surface of the cavity, respectively.

The GSM routine computes the contribution of each part of the cavity surface to the total losses separately assuming that the entire structure is made out of copper with a conductivity $\sigma = 5.8 \cdot 10^7\,\mathrm{S/m}$. The actual losses can then be calculated by individually scaling the copper losses to those of the real materials (superconductor, absorber, steel, ...).

Fig. 14 shows the quality factors of the TM monopole modes of the investigated structure according to Fig. 9 as a function of frequency up to 20 GHz. The solid and the dashed line correspond to a cylindrical cavity approximation with longitudinal orders $n = 0$ and $n > 0$ where this cavity has the same dimensions as one single cell of the TESLA cavity. Most of the resonances are found within the area which is limited by the two lines. This confirms that the quality factors of the investigated structure behave in principle like those of a simple cylindrical cavity which are proportional to $\sqrt{\omega}$. For 20 GHz we expect quality factors in the range between $6 \cdot 10^4$ and $1 \cdot 10^5$.

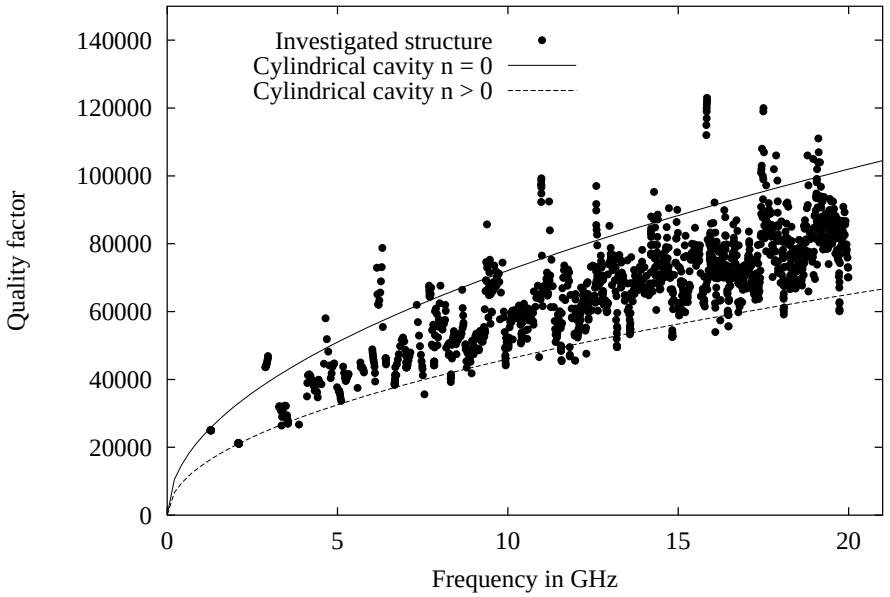

Figure 14: Quality factor of the investigated structure assuming that it is made entirely out of copper.

The eigenmodes of a cavity are not uniformly excited when a bunch traverses the structure. This fact has to be taken into account if one wants to estimate the loss distribution inside the cavity. The excitation of each mode by a δ-bunch is described by the so-called loss parameter. The computation of this quantity was also incorporated in the GSM routine which was used for the calculation of the cavity eigenmodes. Fig. 15 shows the loss parameters as a function of

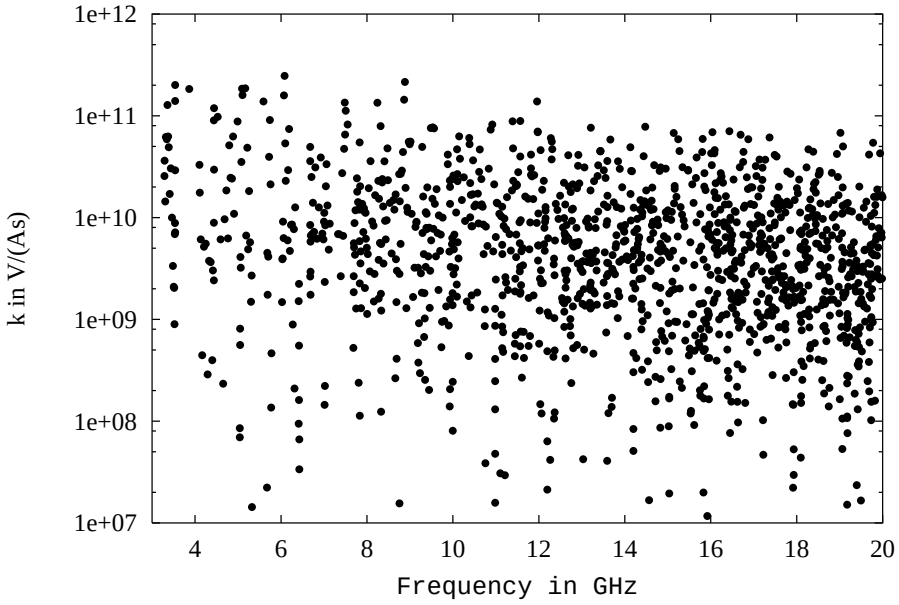

Figure 15: Loss parameter as a function of frequency.

frequency. We will make use of this result in paragraph IIIc).

III Absorber materials

IIIa) Planar model

A simple planar model which is shown in Fig. 16 is employed in order to compare different

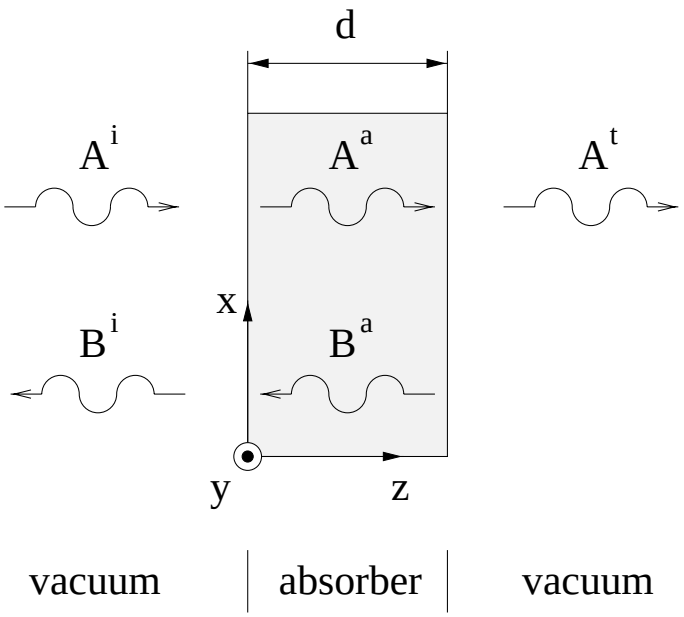

Figure 16: Dielectric slab model of the absorber.

absorber materials. It consists of a dielectric slab (the absorber material) which extends to infinity in the x- and the y-direction. For the sake of simplicity it is assumed that the incident field is a TEM wave propagating in the positive z-direction. This wave is partly reflected and transmitted at the vacuum-material interfaces at $z = 0$ and $z = d$.

Let us define as a figure of merit of an absorber material the quantity η which reads

$$\eta = \frac{P_{loss}}{P_{inc}} \quad . \tag{21}$$

P_{loss} is the power loss in the absorber material; and P_{inc} denotes the power of the incident wave. Thus η can be regarded as something like an absorber efficiency. How P_{loss} can be calculated is shown in the the Appendix.

We need of course a lossy material with a relative large imaginary part of the permittivity for a good absorber efficiency. Nevertheless, a lack of losses can partly be compensated by increasing the absorber thickness in order to have an acceptable η also at low frequencies (30 GHz – 100 GHz). On the other hand, the absorber efficiency at the high frequency end of the considered spectral range (300 GHz – 600 GHz) is basically determined by the real part of the permittivity. If this quantity is large, most of the incident field is reflected at the interface at $z = 0$ and thus cannot be absorbed within the slab. Hence we need a lossy material with a small real part of the permittivity for a highly efficient absorber. E.g., SiC has outstanding large losses ($\varepsilon_r \approx 30$ and $\tan\delta \approx 0.3$ at 20 GHz [15]). Unfortunately the real part of its permittivity is also quite high so that it is not suited as a HOM absorber material.

In order to check that our analysis of the planar model is correct and to see what is the effect of the material parameters (real and imaginary part of the permittivity) on the damping

properties of the absorber let us consider some parameter sets. Fig. 17 shows the electromagnetic

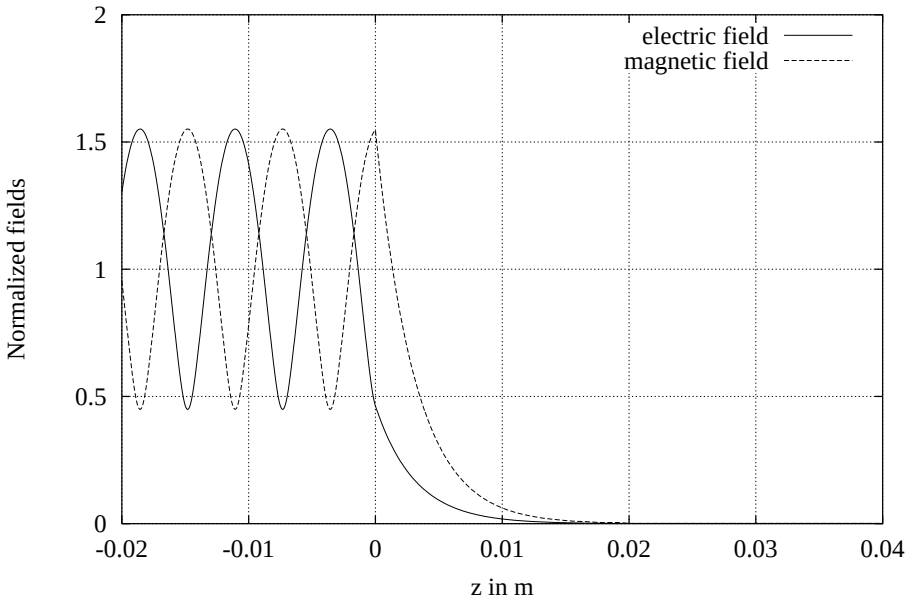

Figure 17: Electromagnetic field as a function of the coordinate normal to the dielectric slab. Parameters: $\varepsilon_r' = 10$, $\varepsilon_r'' = 5$, $d = 2\,\mathrm{cm}$ and $f = 20\,\mathrm{GHz}$.

field as a function of the coordinate normal to the interface of the dielectric slab. For this figure an example absorber with $\varepsilon_r' = 10$ and $\varepsilon_r'' = 5$ is assumed. The frequency of the electromagnetic field is 20 GHz. An absorber with such high losses strongly damps the electromagnetic field. The field within the absorber is exponentially attenuated; and the region behind the absorber is almost field-free. Note that the electric and the magnetic field are continuous at $z = 0$ and $z = d$ which confirms the validity of the analysis.

The corresponding field distributions for an absorber with much lower losses, namely $\varepsilon_r'' = 0.5$, are presented in Fig 18. If we compare Figs. 17 and 18 we clearly see that the absorption of the electromagnetic field is considerably less for the $\varepsilon_r'' = 0.5$ case than for $\varepsilon_r'' = 5$. On the other hand, for $f = 100\,\mathrm{GHz}$, see Fig. 19, $\varepsilon_r'' = 0.5$ is sufficiently high so that the incident field cannot penetrate much into the absorber material.

The field plots in Figs. 17-19 are not suitable to describe the overall performance of an absorber material. Let us therefore consider the absorber efficiency as a function of frequency. Fig. 20 presents the spectral behaviour of η for the two absorber materials which were discussed in Figs. 17-19. As can be concluded from Fig. 20 both materials work well for high frequencies ($f > 30\,\mathrm{GHz}$). The efficiency of the material with $\varepsilon_r'' = 0.5$ is even a little higher than that of the high loss material for $f > 50\,\mathrm{GHz}$ since the reflectivity of the latter material at the interface at $z = 0$ is slightly larger than that of the other one due to its larger ε_r''. However, the performance of the high loss material is much better than that of the material with moderate losses at low frequencies ($f < 20\,\mathrm{GHz}$) where this absorber shows strong oscillations of η due to the frequency dependent interference of the forward and backward propagating waves inside the dielectric slab.

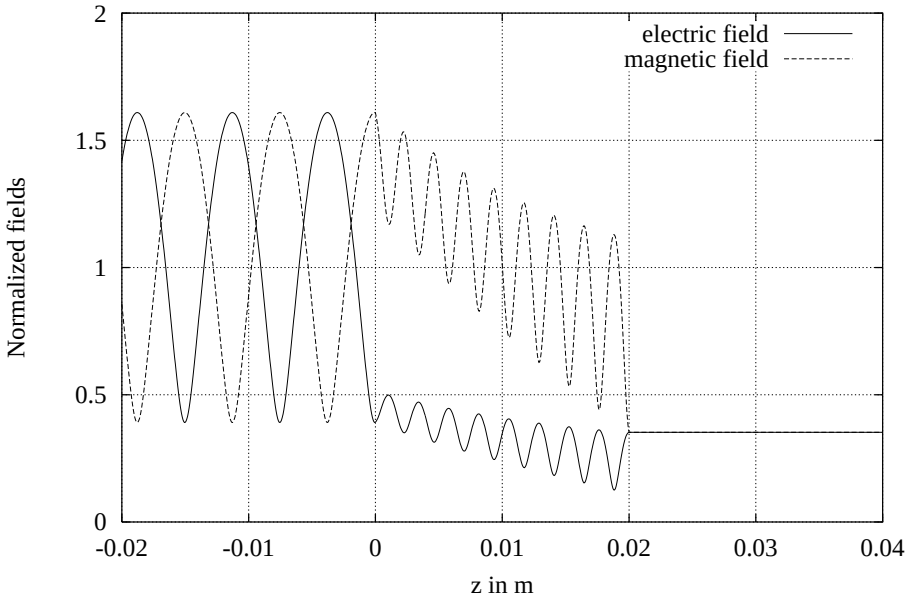

Figure 18: Electromagnetic field as a function of the coordinate normal to the dielectric slab. Parameters: $\varepsilon_r' = 10$, $\varepsilon_r'' = 0.5$, $d = 2\,\mathrm{cm}$ and $f = 20\,\mathrm{GHz}$.

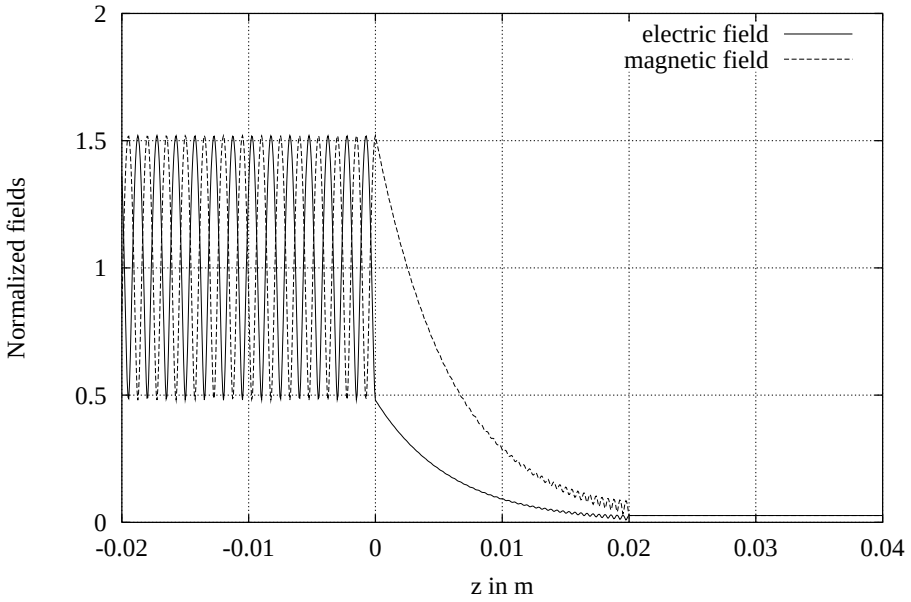

Figure 19: Electromagnetic field as a function of the coordinate normal to the dielectric slab. Parameters: $\varepsilon_r' = 10$, $\varepsilon_r'' = 0.5$, $d = 2\,\mathrm{cm}$ and $f = 100\,\mathrm{GHz}$.

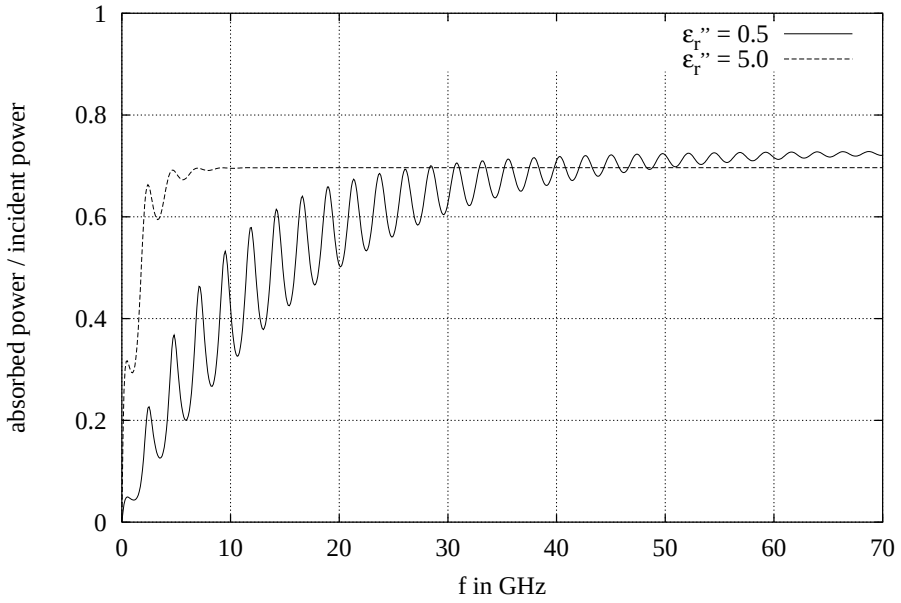

Figure 20: Comparison of the absorber efficiencies corresponding to a material with high losses ($\varepsilon_r'' = 5$) and another one with moderate losses ($\varepsilon_r'' = 0.5$). Parameters: $\varepsilon_r' = 10$, $d = 2\,\mathrm{cm}$.

IIIb) Absorber properties of 0.5AgI*0.5AgPO$_3$ glasses and MACOR

Let us start with a discussion of the absorber properties of 0.5AgI*0.5AgPO$_3$. The conductivity of this glas was measured at the Universität Münster for a variety of temperatures. Unfortunately there is not much information available about this material at 70 K. However, a conductivity spectrum ranging up to about 10 THz was measured at 158 K. In order to illustrate the temperature dependence of the material properties we also consider a corresponding spectrum at 373 K. Both curves are shown in Fig. 21 [16]. The low-frequency range of the 158 K-isotherm includes data taken from [17]. From this figure it can be concluded that the conductivity is approximately temperature independent for $f > 1\,\mathrm{THz}$. On the other hand, σ is much higher for $T = 373\,\mathrm{K}$ than for $T = 158\,\mathrm{K}$ if we consider frequencies less than 100 GHz. The difference between the two curves even amounts to more than five orders of magnitude for $f \to 0$.

Dealing with lossy materials, the losses can either be accounted for by a conductivity σ or an imaginary part of the permittivity. Since we are more used to operate with the complex permittivity we have to translate the conductivity spectra according to Fig. 21 into a corresponding ε'' spectra. From Maxwell's equation

$$\boldsymbol{\nabla} \times \boldsymbol{H} = j\omega\varepsilon\boldsymbol{E} + \sigma\boldsymbol{E} = j\omega\varepsilon_0 \left(\varepsilon_r' + \frac{\sigma}{j\omega\varepsilon_0}\right)\boldsymbol{E} = j\omega\varepsilon_0 \left(\varepsilon_r' - j\varepsilon_r''\right)\boldsymbol{E} \tag{22}$$

it follows that the conductivity σ of a material and the imaginary part of its complex permittivity are related by

$$\varepsilon_r'' = \frac{\sigma}{\omega\varepsilon_0} \quad . \tag{23}$$

The curves which correspond to the conductivity spectra of Fig. 21 are presented in Fig. 22. The increase of ε_r'' for $f \to 0$ is due to the fact that σ becomes frequency independent for low frequencies ($f < 1\,\mathrm{GHz}$ for $T = 373\,\mathrm{K}$ and $f < 10\,\mathrm{kHz}$ for $T = 158\,\mathrm{K}$) and ε_r'' is thus inverse proportional to f according to Eq. (23).

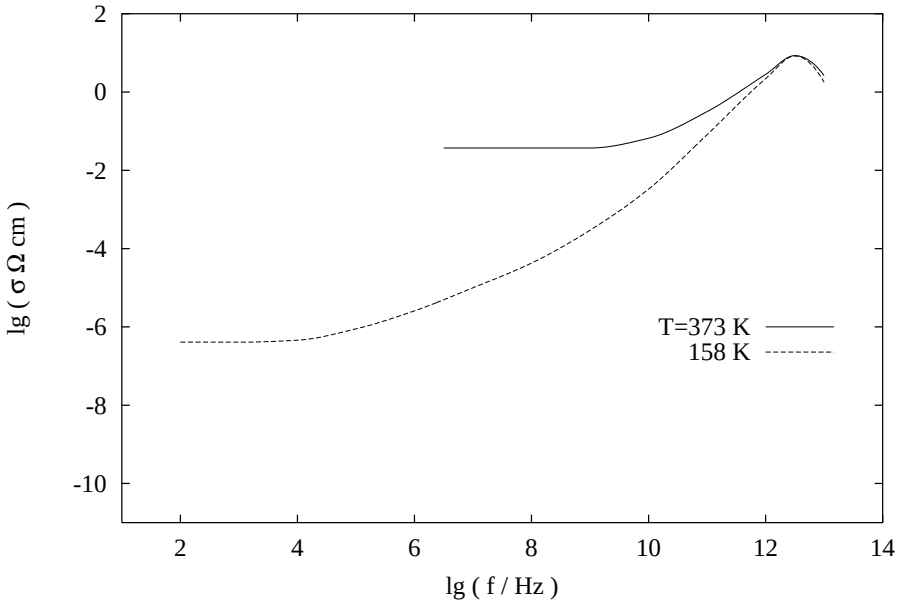

Figure 21: Conductivity of $0.5AgI*0.5AgPO_3$ glasses as a function of frequency with the temperature of the material as a parameter.

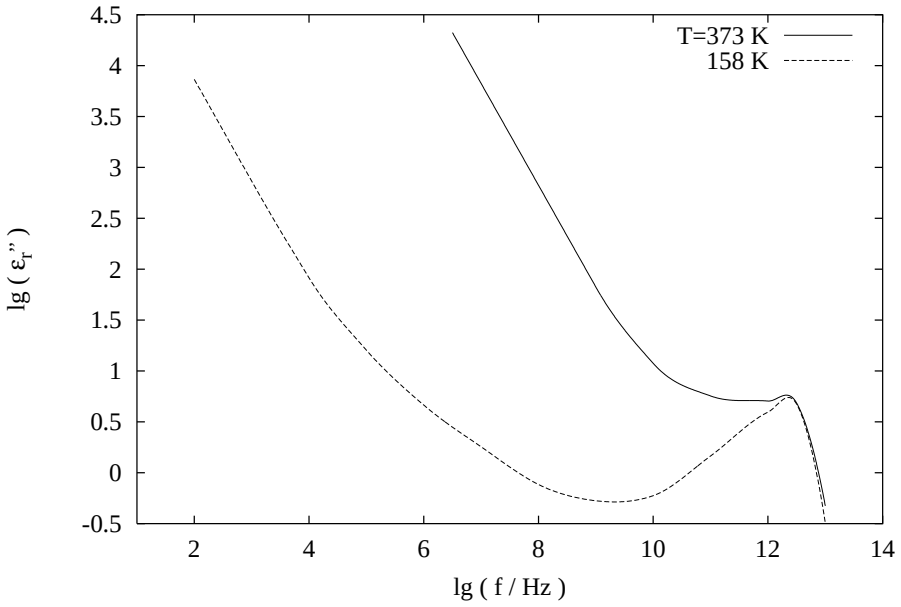

Figure 22: Imaginary part of the relative permittivity of $0.5AgI*0.5AgPO_3$ glasses as a function of frequency with the temperature of the material as a parameter.

Fig. 23 shows the absorber efficiency of $0.5AgI{*}0.5AgPO_3$ for a 5 mm thick slab at a tem-

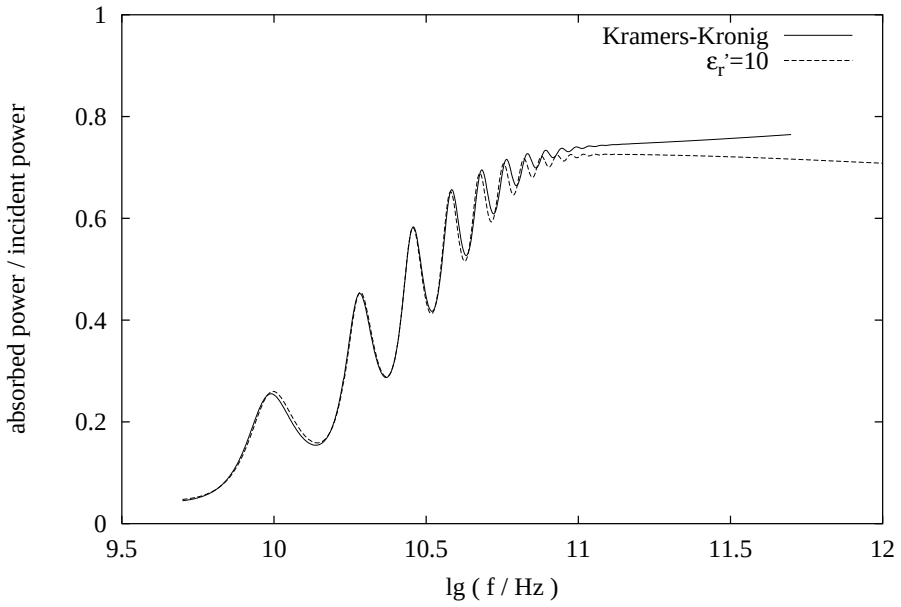

Figure 23: Comparison between the absorber efficiency of $0.5AgI{*}0.5AgPO_3$ glasses if we assume $\varepsilon_r' = 10 \neq f(\omega)$ (dashed line) and if we use the Kramers-Kronig relations in order to determine $\varepsilon_r'(\omega)$ (solid line). Parameters: $T = 158\,\mathrm{K}$, $d = 5\,\mathrm{mm}$.

perature of 158 K. If we assume that $\varepsilon_r' = 10 \neq f(\omega)$, then the dashed line is valid. From the application of the Kramers-Kronig relations it follows however that ε_r' cannot be frequency independent. The solid curve corresponds to the case where we calculated $\varepsilon_r' = f(\omega)$ from $\varepsilon_r''(\omega)$ using the Kramers-Kronig relations. The dashed and the solid line are so close together over the whole frequency range that the simple assumption of $\varepsilon_r' = 10$ seems to be well-justified.

The oscillations of η are getting faster for higher frequencies. Note that this phenomenon may be explained by the logarithmic scale of the frequency axis.

Fig. 24 shows the absorber efficiency of $0.5AgI{*}0.5AgPO_3$ as a function of frequency for various values of d. The temperature of the absorber is 158 K. The electromagnetic field cannot penetrate much into the absorber for high frequencies. Thus all three curves are approximately the same for $f \to \infty$. For $f > 100\,\mathrm{GHz}$, the considerable amount of about 80% of the incident power is absorbed inside the dielectric slab. However, since we are also interested in good damping properties for frequencies down to 30 GHz, the thickness of the absorber material should be even larger than 20 mm. As expected, the oscillations in η are getting faster if the thickness of the absorber slab is increased.

Let us now repeat our analysis with MACOR instead of $0.5AgI{*}0.5AgPO_3$. From [18] and [19] we know the frequency dependence of the complex ε of MACOR at room temperature in the frequency range from 60 GHz to 280 GHz and 150 GHz to 900 GHz, respectively. These results were checked by I. Wilke (Institut für Angewandte Physik, Universität Hamburg) and C. Cramer (Institut für Physikalische Chemie, Universität Münster). Both measurements confirm the values from the literature. Figs. 25 and 26 show the numbers that we have for $\varepsilon_r'(\omega)$ and $\varepsilon_r''(\omega)$. The oscillations in the results of I. Wilke for $\varepsilon_r''(\omega)$ may be explained by the fact that the thickness of her MACOR sample was not known precisely enough. For our further calculations we use the values from [18] and [19].

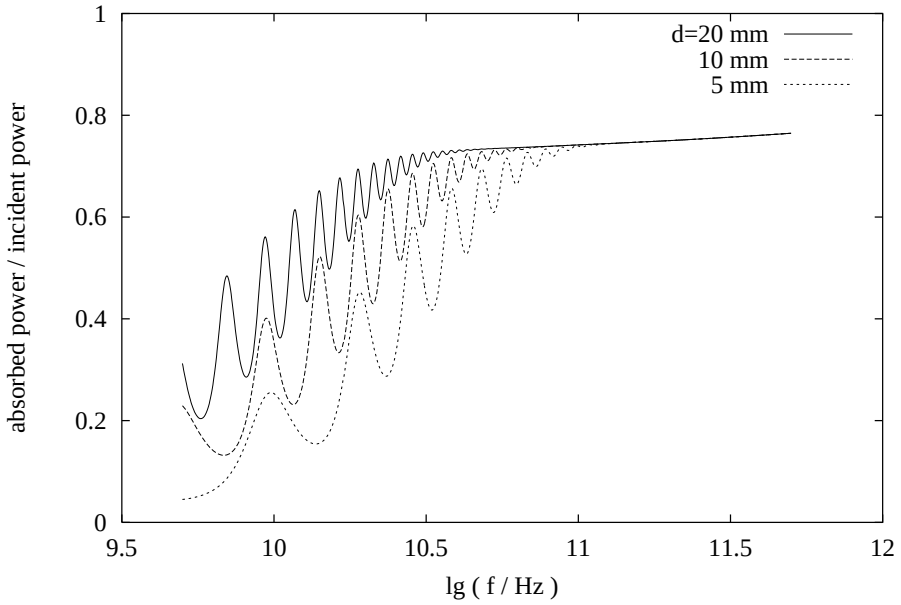

Figure 24: Absorber efficiency of $0.5AgI*0.5AgPO_3$ at 158 K as a function of frequency with the thickness of the dielectric slab as a parameter.

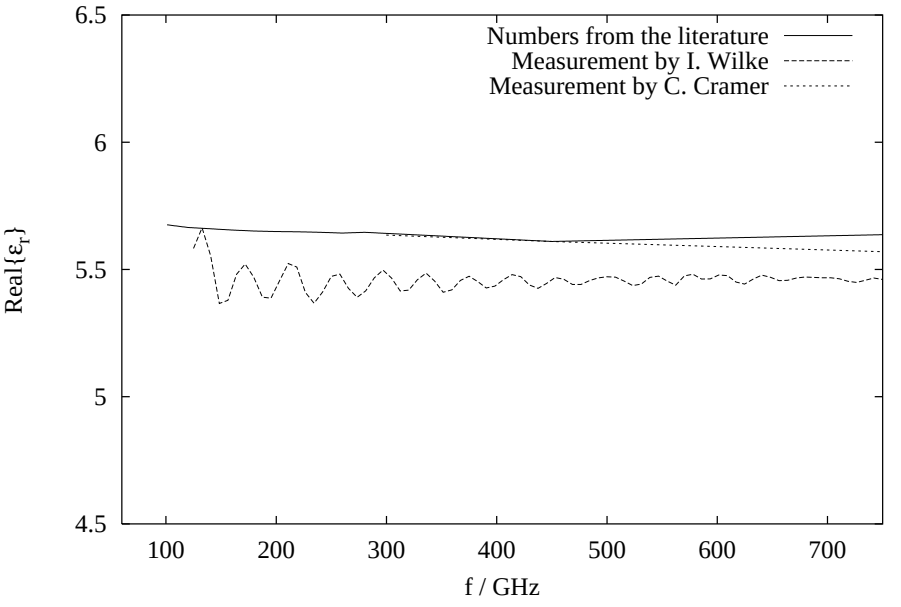

Figure 25: ε'_r of MACOR at room temperature as a function of frequency.

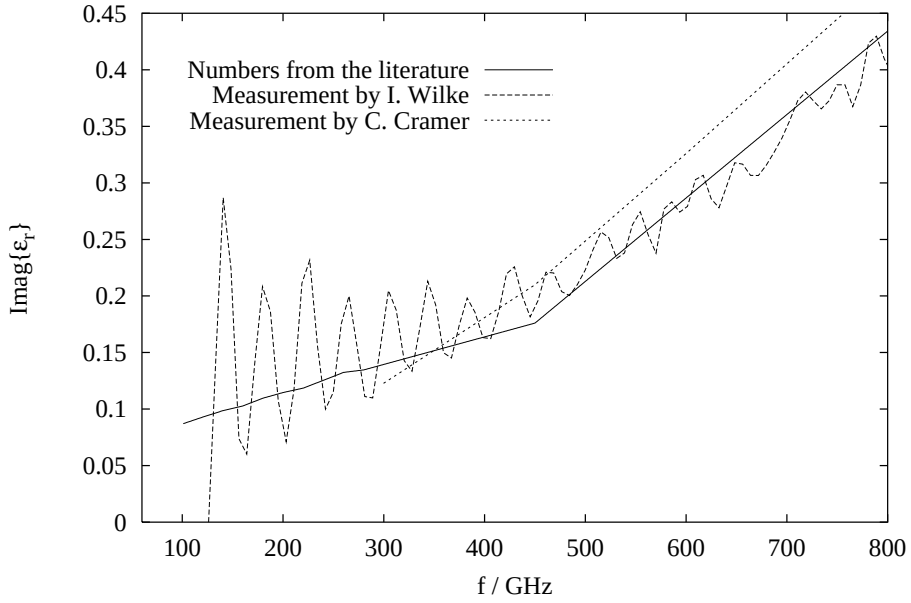

Figure 26: ε_r'' of MACOR at room temperature as a function of frequency.

We also need $\varepsilon_r'(\omega)$ and $\varepsilon_r''(\omega)$ in the range from 3 GHZ to 20 GHz in order to investigate the effect of a MACOR absorber using our modal analysis. Since the functions $\varepsilon_r'(\omega)$ and $\varepsilon_r''(\omega)$ which are given in Figs. 25 and 26 are very smooth we assume that we can extrapolate them to lower frequencies.

A quantity which measures the performance of a material as absorber is the absorber efficiency η which was defined in Eq. (21). Fig. 27 compares η of a MACOR slab at room temperature with that of a $0.5AgI{*}0.5AgPO_3$ slab at 158 K. It is assumed that the thickness of both slabs is 10 mm. The efficiency of the MACOR absorber is even a little higher than that of the $0.5AgI{*}0.5AgPO_3$ slab at the upper part of the considered spectrum ($f > 300$ GHz) because MACOR has the lower real part of the permittivity from both materials. The efficiency of MACOR is on the other hand much less than that of $0.5AgI{*}0.5AgPO_3$ at low and moderate frequencies. This can be explained by the fact that the losses of MACOR are significantly less than those of $0.5AgI{*}0.5AgPO_3$ in this frequency range which follows from comparing the numbers given in Figs. 22 and 26.

If we increase the thickness of the MACOR slab we can considerably enhance the absorber losses at low frequencies. In Fig. 28, a MACOR absorber with $d = 30$ mm is compared with the same $0.5AgI{*}0.5AgPO_3$ absorber that was considered in Fig. 27. The curves show that the frequency at which both materials have the same η reduces from 300 GHz in Fig. 27 to 120 GHz in Fig. 28.

IIIc) The effect of HOM absorbers in a TESLA 9cell structure

The computation of the quality factors in paragrapgh IIc) were done for a cavity which is completely made out of copper. This structure serves us as a reference cavity. Since we are using a perturbation theory for the determination of the quality factors it is possible to calculate the quality factors of the actual structure by simply scaling the copper losses of the individual parts of the cavity.

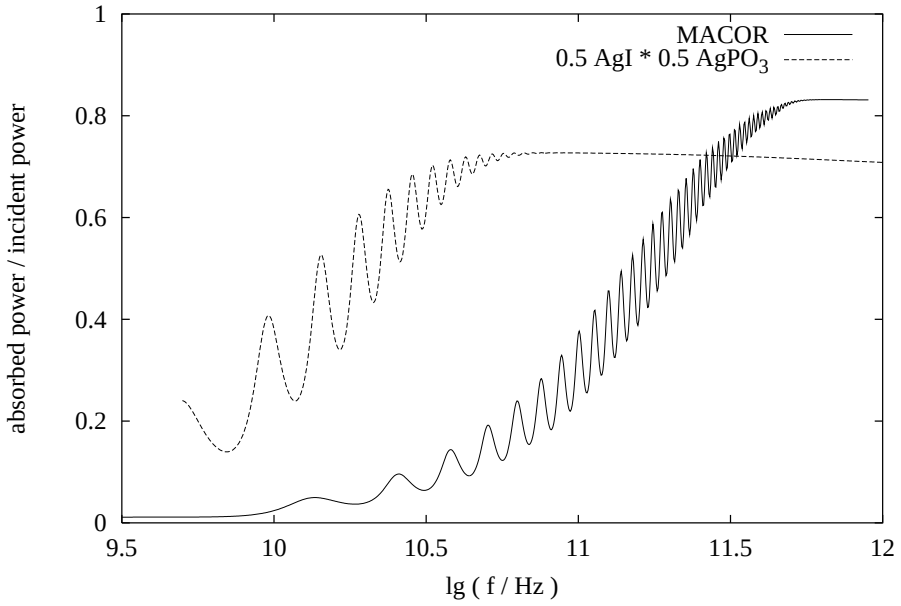

Figure 27: Comparison of the relative absorbed power between a $0.5AgI*0.5AgPO_3$ absorber at 158 K and a MACOR absorber at room temperature. The thickness of the dielectric slab for both types of absorber is 10 mm.

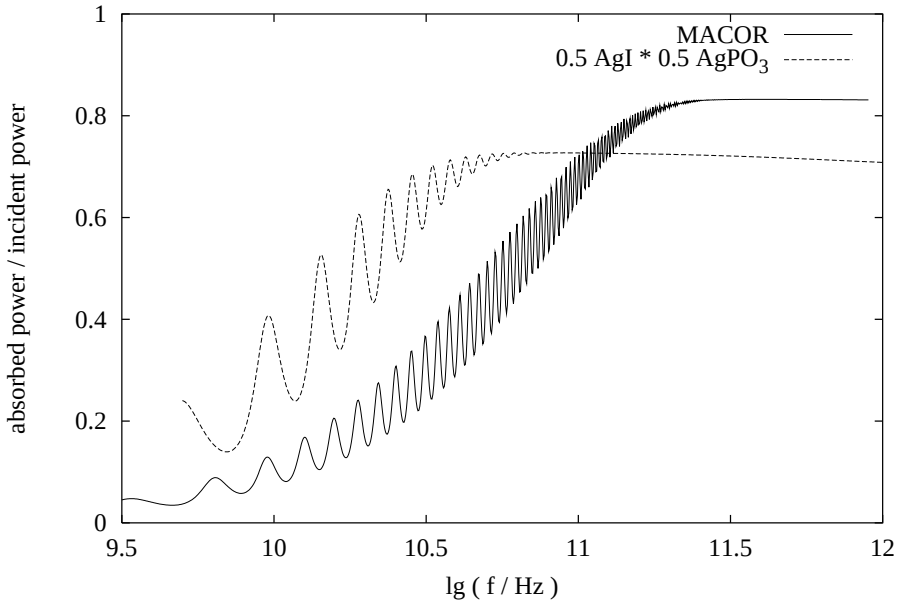

Figure 28: The same comparison between $0.5AgI*0.5AgPO_3$ and MACOR as in Fig. 27 with the exception that the thickness of the MACOR absorber is 30 mm instead of 10 mm.

Let Q^{abs} and Q^{9cell} denote the quality factors corresponding to the absorber cavity and everything of the structure except for this cavity, then the total quality factor of the structure is given by

$$\frac{1}{Q^{tot}} = \frac{1}{Q^{abs}} + \frac{1}{Q^{9cell}} \quad . \tag{24}$$

The scaled quantities of Q^{9cell} and Q^{abs} are marked by a $\tilde{}$. They should be related to the quality factors of the copper structure by

$$\tilde{Q}^{9cell} = \alpha Q^{9cell} \quad , \tag{25}$$

$$\tilde{Q}^{abs} = \beta Q^{abs} \quad . \tag{26}$$

Note that the factors α and β are still unknown and will be determined below. Using Eqs. (25) and (26), the total quality factor of the actual structure reads

$$\frac{1}{\tilde{Q}^{tot}} = \frac{1}{\tilde{Q}^{abs}} + \frac{1}{\tilde{Q}^{9cell}} = \frac{1}{\beta Q^{abs}} + \frac{1}{\alpha Q^{9cell}} \quad . \tag{27}$$

In order to obtain the power ratio $\tilde{P}^{9cell}_{loss}/\tilde{P}^{tot}_{loss}$ let us recall the definitions of the quality factors $\tilde{Q}^{tot}$ and $\tilde{Q}^{9cell}$:

$$\tilde{Q}^{tot} = \frac{W^{tot}}{\omega_0 \tilde{P}^{tot}_{loss}} \quad , \tag{28}$$

$$\tilde{Q}^{9cell} = \frac{W^{tot}}{\omega_0 \tilde{P}^{9cell}_{loss}} \tag{29}$$

In the above equations ω_0 and W^{tot} denote the resonance frequency and the total stored energy in the structure of a specific mode. Dividing Eq. (28) by Eq. (29) and inserting Eq. (27) for $\tilde{Q}^{tot}$, yields

$$\frac{\tilde{P}^{9cell}_{loss}}{\tilde{P}^{tot}_{loss}} = \frac{\tilde{Q}^{tot}}{\tilde{Q}^{9cell}} = \frac{1}{1 + \frac{\alpha Q^{9cell}}{\beta Q^{abs}}} \quad . \tag{30}$$

The ratio $\tilde{P}^{9cell}_{loss}/\tilde{P}^{tot}_{loss}$ gives the power loss of a specific mode in the superconducting part of the structure relative to the total power loss of this mode. Thus, if we initially deposit the energy W_0 in a individual mode of the structure, $\tilde{P}^{9cell}_{loss}/\tilde{P}^{tot}_{loss} \cdot W_0$ is the amount of energy that will be absorbed by the superconducting part of the structure.

The quality factor of a cavity mode is inverse proportional to the real part of the surface impedance of the wall material. Thus α is given by

$$\alpha = \frac{R_{co}}{R_{sc}} \quad , \tag{31}$$

where R_{co} and R_{sc} are the real part of the surface impedance of our copper model and the superconductor, respectively. For R_{co} the well-known relations

$$R_{co} = \frac{1}{\delta_{co}\sigma_{co}} \quad , \quad \delta_{co} = \sqrt{\frac{2}{\omega \mu_0 \sigma_{co}}} \tag{32}$$

hold where σ_{co} and δ_{co} denote the conductivity of copper and the corresponding skin depth. For σ_{co} we assume $5.8 \cdot 10^7$ S/m.

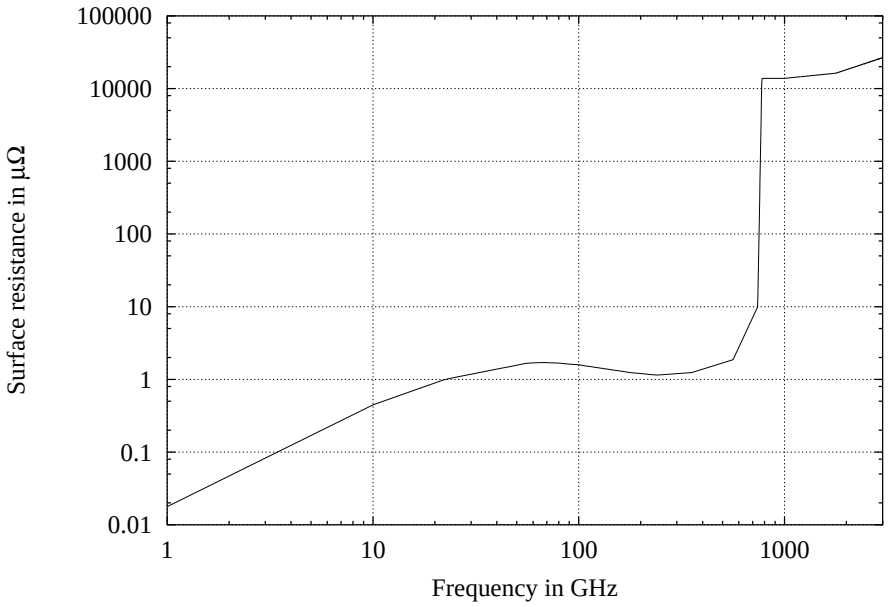

Figure 29: Real part of the surface resistance of niobium at 2 K as a function of frequency.

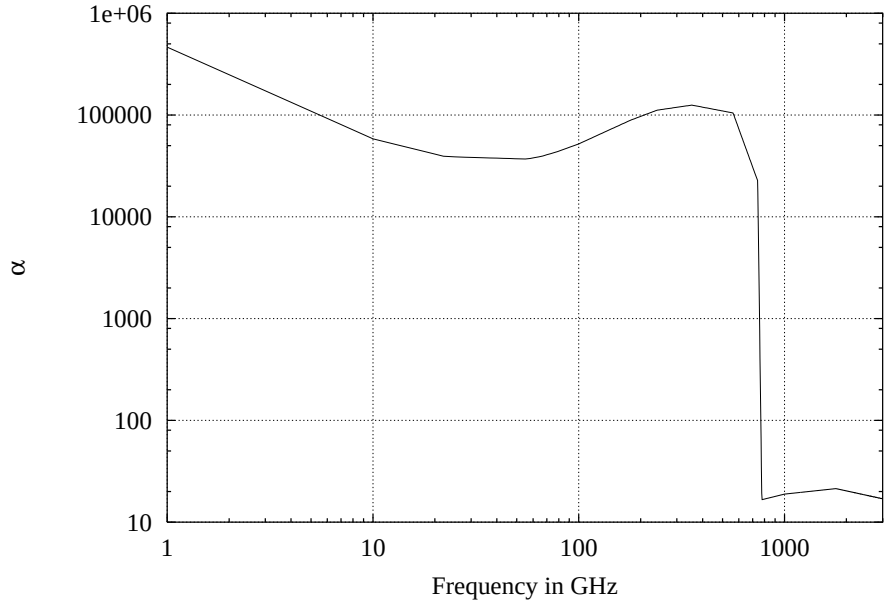

Figure 30: Scaling factor α as a function of frequency.

The real part of the surface resistance of niobium at a temperature of 2 K is shown in Fig. 29. This figure illustrates that the surface resistance increases considerably, by about four orders of magnitude, at a frequency of 700 GHz which is just the threshold for breaking the Cooper pairs. Fig. 30 presents the corresponding scaling factor α as a function of frequency. It is interesting to note that α is still larger than 10 even above the threshold for the break-up of the Cooper pairs. This means that the power loss in a superconducting cavity at a frequency of 1 THz amounts only to 1/10 of that corresponding to a copper cavity at room temperature.

It still remains to determine the scaling factor β according to Eq. (26) for the actual absorber cavity. Let us start our analysis with the intrinsic beam impedance of copper:

$$Z_{co} = \sqrt{\frac{\mu_0}{\varepsilon}} = \sqrt{\frac{\mu_0}{\varepsilon_0 \left(1 - j\frac{\sigma}{\omega\varepsilon_0}\right)}} \tag{33}$$

The above equation may be simplified due to the large conductivity of copper:

$$Z_{co} \approx \sqrt{\frac{j\omega\mu_0}{\sigma}} \tag{34}$$

The reflection coefficient of a TEM wave which is normally incident on a vacuum-copper interface reads

$$r = \frac{Z_{co} - Z_0}{Z_{co} + Z_0} \quad . \tag{35}$$

The power which is absorbed by the copper relative to the power of the incident wave can be calculated by

$$\eta_{co} = 1 - |r|^2 \quad . \tag{36}$$

The quantity η_{co} can then be compared with the absorber efficiency η according to Eq. (21) which was used as a figure of merit for an absorber material in the planar model. The scaling factor β is therefore given by

$$\beta = \frac{\eta_{co}}{\eta} \quad . \tag{37}$$

Fig. 31 shows this quantity as a function of frequency. The typical oscillations of η in the low frequency range which we know already from Fig. 24 can also be recognized in this figure. Nevertheless, in the whole frequency range from 1 GHz to 3 THz, which is shown in Fig. 31, β stays significantly below 0.01.

Fig. 32 presents the relative power absorption of each individual cavity mode in the superconducting part of the investigated structure according to Eq. (30). For the absorber we have assumed the same parameters as those which were used for Fig. 31. $\widetilde{P}_{loss}^{9cell} / \widetilde{P}_{loss}^{tot}$ of most of the modes is below 1%. This means that more than 99% of the energy of each mode is absorbed by the HOM absorber.

On the other hand, a few modes exist where the energy is almost completely lost outside the absorber. Fig. 33 shows the axial electric field of such a mode as a function of the axial coordinate. The energy of this mode is closely bound to the beampipe at the left-hand-side of the structure. Such modes are therefore called beampipe modes. Hence the absorber which is located at the other side of the structure does not "see" the electromagnetic field of this mode and can consequently not attenuate it. However, these beampipe modes have been artificially introduced by our model which requires short circuits at both ends of the structure so that we should not worry about them.

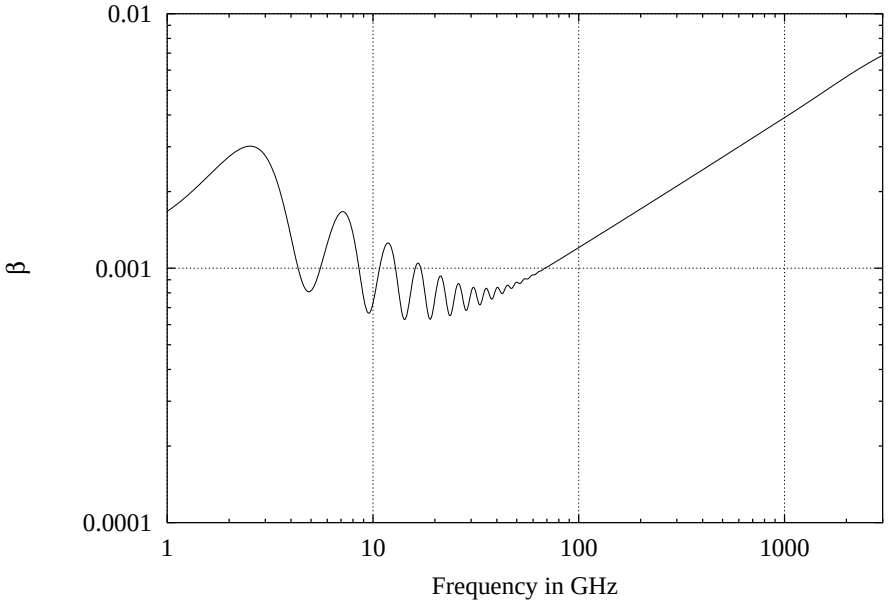

Figure 31: Scaling factor β as a function of frequency. As absorber we have assumed $0.5AgI*0.5AgPO_3$ at a temperature of 158 K and with a thickness of 10 mm.

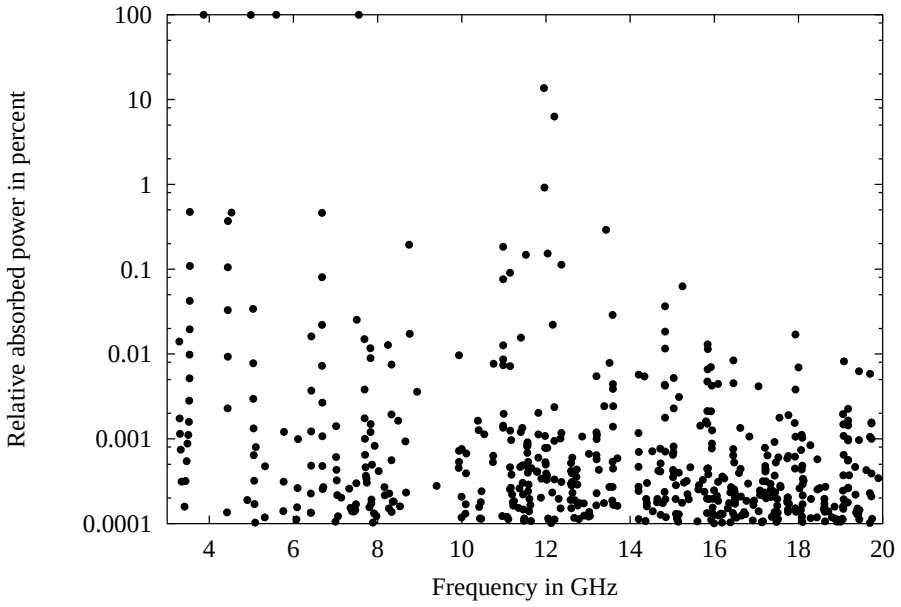

Figure 32: Relative power absorption of each individual cavity mode in the superconducting part of the investigated structure in the presence of a $0.5AgI*0.5AgPO_3$ absorber.

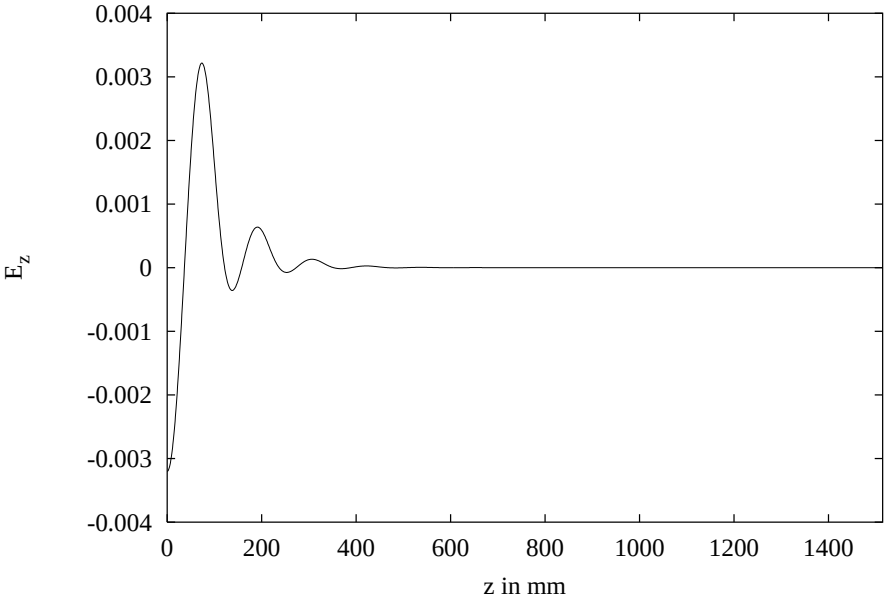

Figure 33: Axial electric field of a beampipe mode ($f = 3.8681\,\mathrm{GHz}$) as a function of the axial coordinate.

Up to this point of the analysis we have not taken into account that the modes are not uniformly excited by a bunch. The energy which a δ-bunch excitation deposits in the ith mode is proportional to the loss parameter k_i of this mode. Since we computed the mode spectrum only to an upper frequency limit of 20 GHz we can actually assume that the structure is excited by a δ-bunch. The quantity ξ which is defined as

$$\xi = \frac{\sum_{i=1}^{N} \frac{\widetilde{P}^{9cell}_{loss,i}}{\widetilde{P}^{tot}_{loss,i}} k_i}{\sum_{i=1}^{N} k_i} \tag{38}$$

describes how much of the total energy which the bunch has lost after it traversed the structure ($\sum_{i=1}^{N} k_i$) is absorbed by the superconducting part of the structure ($\sum_{i=1}^{N} \frac{\widetilde{P}^{9cell}_{loss,i}}{\widetilde{P}^{tot}_{loss,i}} k_i$). Using the numbers for $\frac{\widetilde{P}^{9cell}_{loss,i}}{\widetilde{P}^{tot}_{loss,i}}$ from Fig. 32 and the loss parameters k_i from Fig. 15, we obtain ξ as a function of the frequency limit up to which cavity modes are taken into account as shown in Fig. 34. The steep increase of ξ at about 12 GHz is due to the two modes with a relatively high value of $\frac{\widetilde{P}^{9cell}_{loss,i}}{\widetilde{P}^{tot}_{loss,i}}$ ($\approx 10\%$) which can also be recognized in Fig. 32. However the curve levels out at a value of less than 0.03%. Consequently it seems that we may get rid of almost all of the HOM energy using such an $0.5\mathrm{AgI}^{*}0.5\mathrm{AgPO}_3$ absorber.

Fig. 35 shows the values for ξ according to Eq. (38) for MACOR absorbers with $d = 10\,\mathrm{mm}$ and $d = 30\,\mathrm{mm}$ as a function of the frequency up to which cavity eigenmodes are taken into account in order to compute ξ. Both curves have again a step at 12 GHz which we know already from Fig. 34. The curve for the absorber with a thickness of 30 mm levels out at a significantly lower value ($\approx 0.05\%$) than that corresponding to the 10 mm absorber ($\approx 0.13\%$). However, both curves are much less than 10%, which still would be acceptable, although the absorber efficieny of MACOR is relatively low in the frequency range up to 20 GHz according to Figs. 27

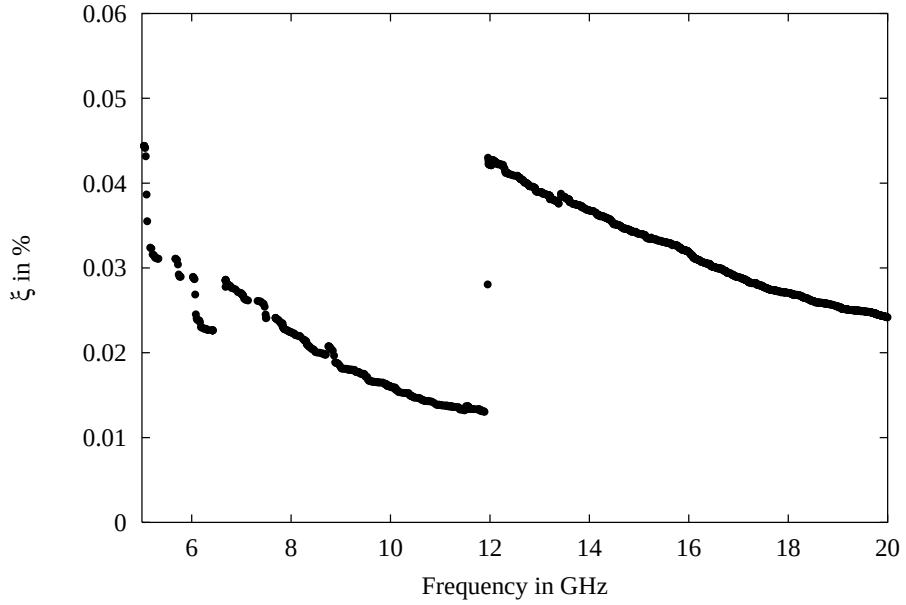

Figure 34: Relative power absorption in the superconducting part of the investigated structure as a function of the frequency limit up to which cavity modes are taken into account.

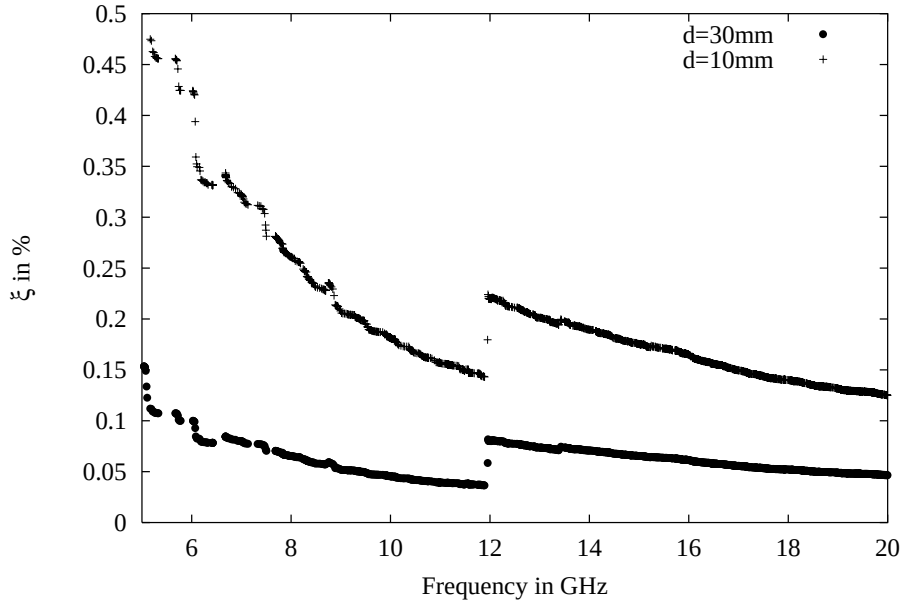

Figure 35: Comparison of ξ for a MACOR absorber with a thickness of 10 mm and 30 mm.

and 28. Hence a MACOR absorber with a thickness which is even less than 10 mm could be used.

We have to keep in mind that we assumed the material properties of MACOR at room temperature as input data for our simulations. The actual HOM absorber will however be used at a temperature level of about 70 K. Moreover we will have only one absorber per module (and not per cavity) in TESLA; and there will also be some normal conducting elements (input coupler, low-frequency HOM coupler, shutters, ...) at 2 K and 4 K. From some preliminary measurements we estimate that the reduced absorber temperature leads to an increase of ξ by a factor of 5; and the fact that there will be only one absorber per module can roughly be taken into account by multiplying ξ with another factor of 10. This results in a value for ξ at 20 GHz for the 30 mm absorber of about 2.5% which is more than sufficient. However, the absorption of the normal conducting components which is not included in this number has still to be checked.

IV Measurements in a 9cell copper cavity

IVa) Experimental setup

The experimental setup which is shown in Fig. 36 consists basically of a HP8720C VNA, an automatic calibration set (ECal) and the copper model of a TESLA 9cell cavity with attached absorber cell including absorber material and an antenna which is used to excite the structure.

The VNA covers a frequency range from 50 MHz to 20 GHz. During the measurements the results are temporarily stored on an external hard disc and after transfered to a workstation for the numerical evaluation of the raw data.

In Fig. 36, the device on top of the VNA is the ECal control unit. The small box in front of the structure contains the required calibration standards. Before measuring the actual input reflection of the device under test a calibration has to be done for each specific VNA setting (frequency range, resolution etc.).

Fig. 37 presents a detailed view of the absorber cavity which is attached to the TESLA 9cell cavity through a flange. A coaxial antenna transition which is sketched in Fig. 38 is used to excite the system for the measurement of the input reflection.

Any waveguide mode that has nonzero electric field along the probe excites currents on the probe antenna. By reciprocity, when the probe current is produced by a TEM wave incident from the coaxial line, the same waveguide modes are excited. In our case these are the TM monopole modes.

In order to avoid distortion due to unwanted antenna resonances, the antenna length has to be significantly smaller than the free-space wavelength which is 15 mm for a frequency of 20 GHz. The shortest probe that we used had a length of only 2 mm. The coupling to most of the cavity modes is however very small for such a short probe. Thus we also used a 5 mm antenna in the frequency range up to 10 GHz.

Fig. 39 shows the dismantled absorber cavity. From this figure one can recognize how the MACOR pipe is supported inside the cavity. Inner and outer diameter of the absorber are 88 mm and 108 mm, respectively. The diameter of the beampipe is 10 mm smaller than the inner diameter of the absorber pipe. The cavity has an outer diameter of 128 mm so that also absorbers with a larger wall thickness than the shown MACOR pipe may be tested.

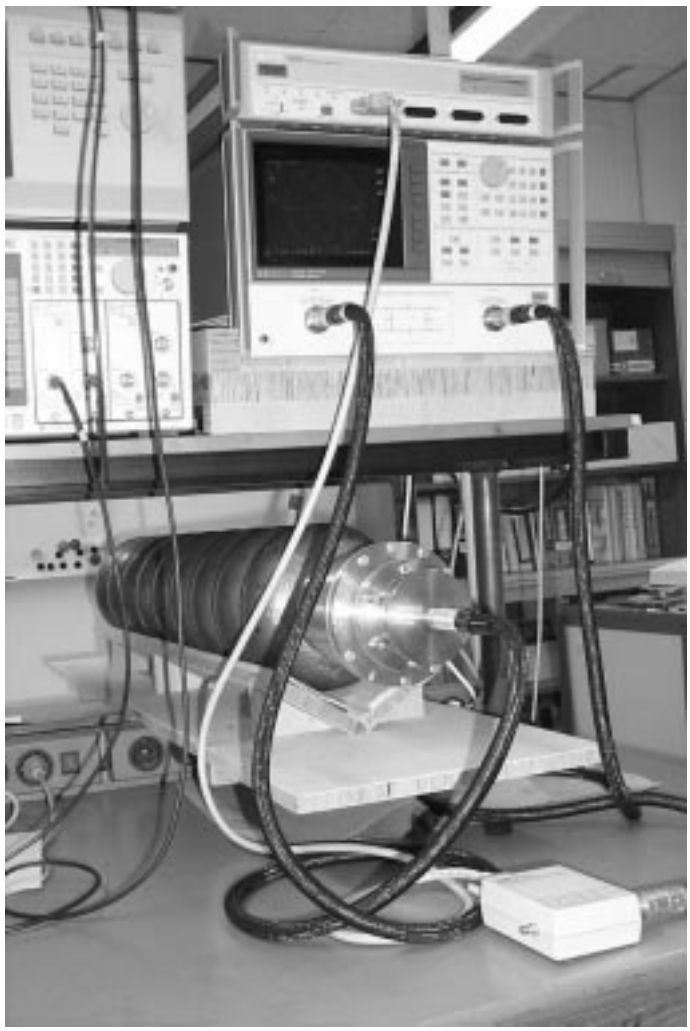

Figure 36: Experimental setup consisting of a VNA, a corresponding calibration set and a copper model of a TESLA 9cell structure to which the absorber cavity is already connected.

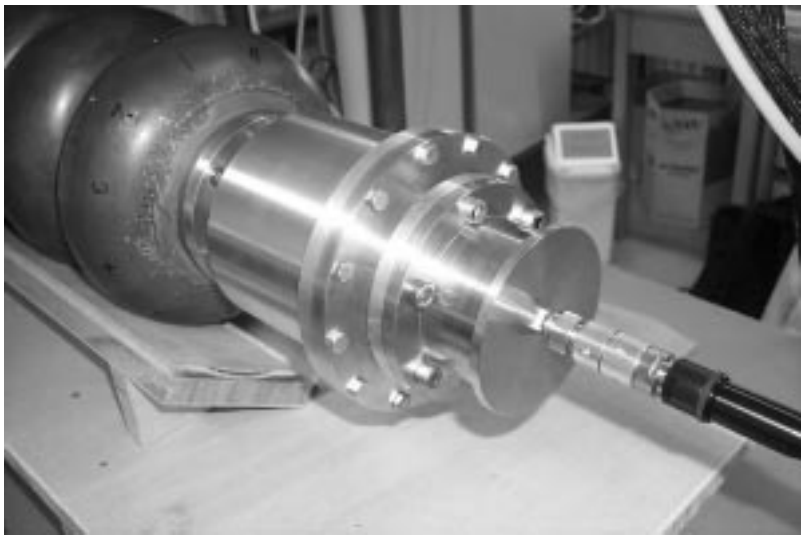

Figure 37: Detailed view of the absorber cavity.

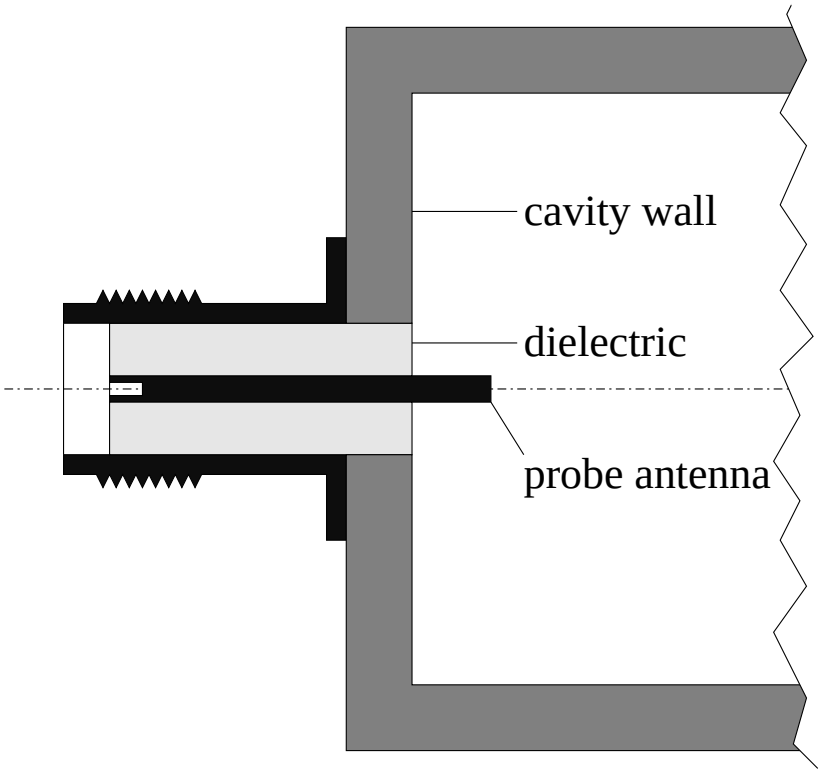

Figure 38: Schematics of the coaxial antenna transition.

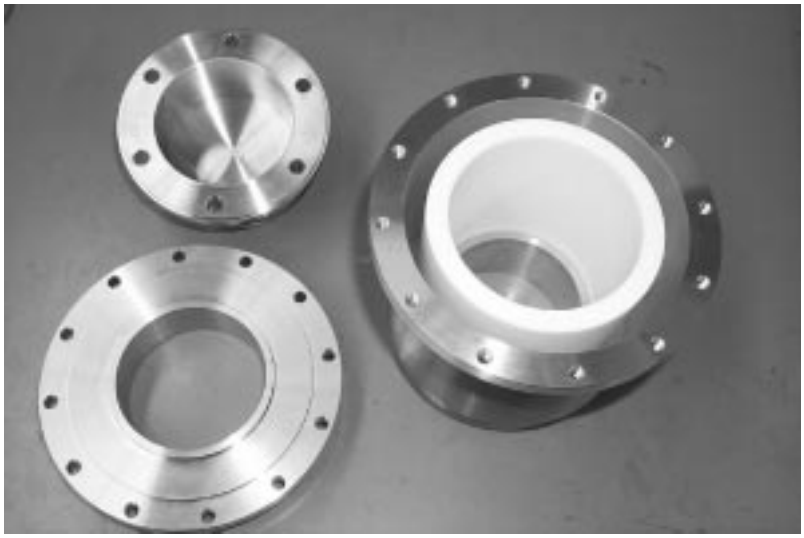

Figure 39: Dismantled absorber cavity.

IVb) Calculation of the internal quality factors from the input reflection

As mentioned the input reflection of the test cavity is measured using a VNA. But how can we calculate the quality factor of a resonant mode from the measured input reflection?

In order to answer this question we have to keep in mind that the spectral density of the resonances in the 9cell cavity is considerably high in the investigated frequency range from 3 GHz to 20 GHz. This means that even if one mode is tuned close to its resonance so that it dominates the frequency dependence of the input impedance of the cavity the influence of all other modes which contribute parasiticly to this quantity cannot be neglected.

Hence the following model for the input impedance Z is used:

$$Z = \frac{C}{j\omega - p} + D \tag{39}$$

The above formula is valid for angular frequencies ω close to the resonant frequency ω_0 of an individual mode which is identical to the imaginary part of the complex eigenvalue p:

$$p = j\omega_0 \left(1 + j\frac{1}{2Q}\right) \tag{40}$$

Cavity losses are taken into account by the quality factor Q. Thus the real part of p is equal to $-\omega_0/2Q$.

There are two further constants C and D in Eq. (39). C is a real number; whereas D can be assumed as purely imaginary. This can be explained in the following way: The constant D is used to take the effect of the parasitic modes into account. So if we consider a well-isolated resonance which allows us to neglect the influence of all other modes ($D = 0$) and if we assume that the considered mode is lossless ($Q \to \infty$), the corresponding input impedance can be

written as

$$Z = \frac{C}{j\,(\omega - \omega_0)} \tag{41}$$

according to Eqs. (39) and (40). Since we know that the input impedance of a lossless structure is purely imaginary it is obvious that C has to be real.

In order to demonstrate that the real part of D is negligible let us consider the input impedance of a single mode as a function of $\Delta\omega$ which is just $\omega - \omega_0$. From Eqs. (39) and (40) it follows

$$Z = -C\frac{\mathrm{Re}\{p\} + j\Delta\omega}{(\mathrm{Re}\{p\})^2 + \Delta\omega^2} \quad . \tag{42}$$

Assuming that $\Delta\omega \gg \mathrm{Re}\{p\}$, which is in general valid for the parasitic modes in the considered frequency range, Z can be approximated as

$$Z \approx -C\left(\frac{\mathrm{Re}\{p\}}{\Delta\omega^2} + j\frac{1}{\Delta\omega}\right) \quad . \tag{43}$$

Note that the real part of Z is proportional to $1/\Delta\omega^2$; whereas the imaginary part of Z shows a $1/\Delta\omega$-dependence. Since the previously made assumption $\Delta\omega \gg \mathrm{Re}\{p\}$ already implies that the real part of Z is much less than its imaginary part, it is clear that the constant D which summarizes the effect of all parasitic modes is dominated by its imaginary part.

The reflection coefficient which corresponds to the input impedance Z reads

$$R = \frac{Z-1}{Z+1}e^{j\varphi} \quad . \tag{44}$$

The factor $e^{j\varphi}$ is necessary because the location of the reference plane at the cavity entrance which is defined by an input reflection coefficient according to Eq. (44) with $\varphi = 0$ is not known. Inserting Z according to Eq. (39) into the formula for the reflection coefficients, yields

$$R = e^{j\varphi}\frac{D-1}{D+1}\frac{\left(\frac{C}{D-1} - p\right) + j\omega}{\left(\frac{C}{D+1} - p\right) + j\omega} \quad . \tag{45}$$

This reflection coefficient tends to

$$R_{inf} = e^{j\varphi}\frac{D-1}{D+1} \tag{46}$$

if $\omega \to \infty$. It is worth noting that the factor $(D-1)\,/\,(D+1)$ can be written as

$$\frac{D-1}{D+1} = e^{j\Psi} \tag{47}$$

because it was assumed that D is purely imaginary. This means that concerning R_{inf} the effect of the parasitic modes is the same as a transmission line in front of the cavity which leads to a phase shift Ψ of the input reflection. If we normalize R to R_{inf}, Eq. (45) becomes

$$\frac{R}{R_{inf}} = \frac{\left(\frac{C}{D-1} - p\right) + j\omega}{\left(\frac{C}{D+1} - p\right) + j\omega} \quad . \tag{48}$$

Eq. (48) represents a bilinear transformation. If we introduce the abbreviations

$$A = \frac{C}{D-1} - p \quad , \tag{49}$$

$$B = \frac{C}{D+1} - p \quad , \tag{50}$$

Eq. (48) can be reformulated as

$$\frac{R}{R_{inf}} = \frac{A + j\omega}{B + j\omega} \quad . \tag{51}$$

From the fact that

$$\lim_{\omega \to \infty} \frac{d}{d\omega} \frac{R}{R_{inf}} = \text{purely imaginary} \tag{52}$$

it follows immediately that the imaginary parts of the complex constants A and B are identical:

$$\mathrm{Im}\{A\} = \mathrm{Im}\{B\} \tag{53}$$

For convenience, let us define the frequency ω_1 as

$$\omega_1 = -\mathrm{Im}\{A\} = -\mathrm{Im}\{B\} \quad . \tag{54}$$

Then R/R_{inf} reads

$$\frac{R}{R_{inf}} = \frac{\mathrm{Re}\{A\} + j\,(\omega - \omega_1)}{\mathrm{Re}\{B\} + j\,(\omega - \omega_1)} \quad . \tag{55}$$

For the time being let us assume that A and B are already known. Then it still remains to calculate the parameters of the impedance model from these quantitities. For the real parts of A and B we get

$$\mathrm{Re}\{A\} = \mathrm{Re}\left\{\frac{C}{D-1} - p\right\} = -\frac{C}{1 + (\mathrm{Im}\{D\})^2} - \mathrm{Re}\{p\} \quad , \tag{56}$$

$$\mathrm{Re}\{B\} = \mathrm{Re}\left\{\frac{C}{D+1} - p\right\} = \frac{C}{1 + (\mathrm{Im}\{D\})^2} - \mathrm{Re}\{p\} \quad . \tag{57}$$

Adding and substracting Eqs. (56) and (57), yields

$$\mathrm{Re}\{p\} = -\frac{1}{2}\left(\mathrm{Re}\{A\} + \mathrm{Re}\{B\}\right) \quad , \tag{58}$$

$$C = \frac{1 + (\mathrm{Im}\{D\})^2}{2}\left(\mathrm{Re}\{B\} - \mathrm{Re}\{A\}\right) \quad . \tag{59}$$

The corresponding relations for the imaginary parts of A and B are

$$\mathrm{Im}\{A\} = \mathrm{Im}\left\{\frac{C}{D-1}\right\} - \omega_0 \quad , \tag{60}$$

$$\mathrm{Im}\{B\} = \mathrm{Im}\left\{\frac{C}{D+1}\right\} - \omega_0 \quad . \tag{61}$$

Eqs. (60) and (61) confirm that our previous statement $\mathrm{Im}\{A\} = \mathrm{Im}\{B\}$ is correct. Thus we actually get only one equation from the imaginary parts of A and B which reads

$$\omega_0 = \omega_1 - C\frac{\mathrm{Im}\{D\}}{1 + (\mathrm{Im}\{D\})^2} \tag{62}$$

if we use ω_1 instead of $-\mathrm{Im}\{A\}$ according to Eq. (54). Eq. (58) means that the real part of the eigenvalue p is well-defined. On the other hand, the impedance model parameters C and D are not fully determined by the input reflection: For any given D, C and ω_0 may be calculated from Eqs. (59) and (62), respectively. Nevertheless, we can assume with good accuracy that each ω_0

is very close to a minimum of $|R(\omega)|$. Thus the internal quality factor of a resonance, which is the quantity we are interested in, is given by

$$Q = \frac{\omega_0}{\mathrm{Re}\{A\} + \mathrm{Re}\{B\}} \quad . \tag{63}$$

We must keep in mind that we still have to determine the complex constants A and B. If R_{inf} is known, this can easily be done using two frequency points of $R(\omega)$ in the vicinity of a minimum of $|R(\omega)|$:

$$A - \frac{R(\omega_i)}{R_{inf}} B = j\omega_i \left(1 - \frac{R(\omega_i)}{R_{inf}}\right) \quad \text{with} \quad i = 1, \ldots, N \quad \text{and} \quad N \geq 2 \tag{64}$$

Eq. (64) leads to a 2×2 linear system of equations. If necessary more than 2 frequency points can be taken into account in order to minimize the effect of measurement errors.

The construction of R_{inf} is based on the following concept: The input reflection which corresponds to a single resonance is a perfect circle which touches the periphery of the Smith chart at R_{inf}. The influence of the parasitic modes leads to a deformation of this circle. Fig. 40 shows a typical example for such a curve $R(\omega)$ which is quite different from that what we expect

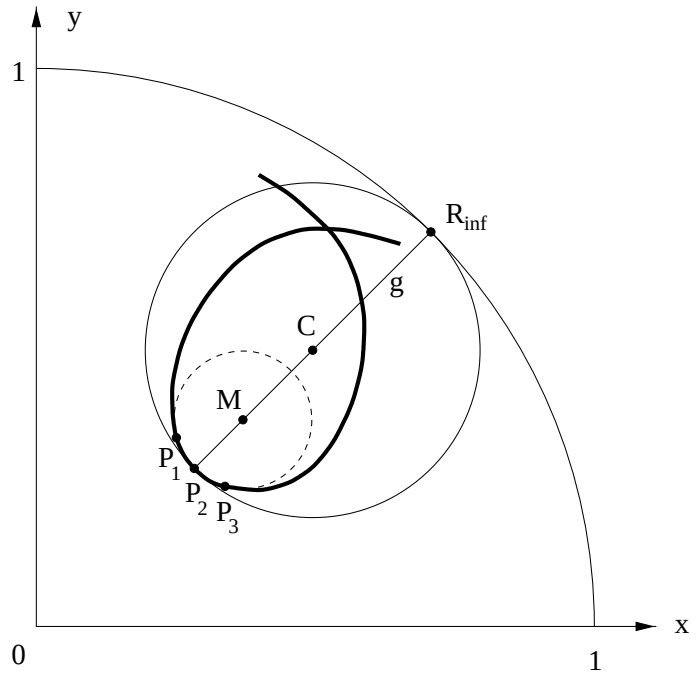

Figure 40: This Fig. illustrates the determination of R_{inf} from the input reflection in the complex plane.

for a single resonance. Nevertheless, we may assume that the direction of the curvature of $R(\omega)$ at its minimum is still more or less the same than that of the corresponding single resonance curve what we are looking for. Then it is obvious that the centre of the circle which describes this single resonance is located somewhere on the line g which is given by

$$\begin{pmatrix} g_x \\ g_y \end{pmatrix} = \begin{pmatrix} r_x \\ r_y \end{pmatrix} + \begin{pmatrix} s_x \\ s_y \end{pmatrix} \xi \quad , \tag{65}$$

where r_x and r_y are the x- and y-coordinates of P_2 and the vector $(s_x, s_y)^t$ reads

$$\begin{pmatrix} s_x \\ s_y \end{pmatrix} = \begin{pmatrix} m_x - r_x \\ m_y - r_y \end{pmatrix} \quad . \tag{66}$$

The coordinates m_x and m_y correspond to the centre of the circle which is uniquely defined by the three points P_1, P_2 and P_3. The parameter ξ which corresponds to the centre of the equivalent single resonance circle C lies somewhere in between $0 < \xi < \xi_{max}$ where ξ_{max} is determined by

$$g_x^2 + g_y^2 = 1 \quad . \tag{67}$$

The evaluation of Eq. (67) leads to

$$\xi_{mx} = -\frac{r_x s_x + r_y s_y}{s_x^2 + s_y^2} + \sqrt{\left(\frac{r_x s_x + r_y s_y}{s_x^2 + s_y^2}\right)^2 + \frac{1 - \left(r_x^2 + r_y^2\right)}{s_x^2 + s_y^2}} \quad . \tag{68}$$

On the other hand, the equivalent single resonance circle touches the periphery of the Smith chart at R_{inf} which is given by the coordinates p_x and p_y in the xy-plane. Assuming that the centre of the circle, the coordinates of which are denoted by c_x and c_y, is known, p_x and p_y may be calculated from

$$p_x = \frac{c_x}{\sqrt{c_x^2 + c_y^2}} \quad , \tag{69}$$

$$p_y = \frac{c_y}{\sqrt{c_x^2 + c_y^2}} \quad . \tag{70}$$

The centre of the circle is actually defined by the fact that P_2 is also a point on the circle. This means that the distance from the centre to R_{inf} is equal to that between the centre and P_2:

$$\rho_1 = \rho_2 \quad \text{with} \tag{71}$$

$$\rho_1 = \sqrt{(p_x - c_x)^2 + (p_y - c_y)^2} \quad , \tag{72}$$

$$\rho_2 = \sqrt{(r_x - c_x)^2 + (r_y - c_y)^2} \tag{73}$$

The coordinates c_x and c_y are computed numerically. A program was written which varies c_x and c_y until $|\rho_1 - \rho_2| < 10^{-10}$ is reached. The routine starts with c_x and c_y corresponding to $\xi_{max}/2$ as an initial guess.

Fig. 41 shows a typical example for the input reflection of the 9cell copper cavity in the vicinity of a resonance. The minimum input reflection is found at $f_{res} = 3.996390\,\text{GHz}$. For this measurement, 801 frequency points were recorded; and the intermediate bandwidth Δf_i was set to 3000 Hz. Even if we use this relatively large value for Δf_i in order to reduce the time which is required for the measurement, the signal to noise ratio of the curve is still quite well. Significant noise is only observed far away from the resonance where $|r(\omega)|$ is close to 1. However, this noise does not hurt us because the procedure for the determination of the internal quality factor only makes use of frequency points in the immediate vicinity of the minimum.

Fig. 42 presents the input reflection in the complex plane. The measured curve which is given by the solid line looks like a perfect circle which touches the periphery of the Smith chart. This resonance behaves therefore like a single well-isolated mode for which the influence of parasitic modes can be neglected. The dots indicate the single mode resonance curve which

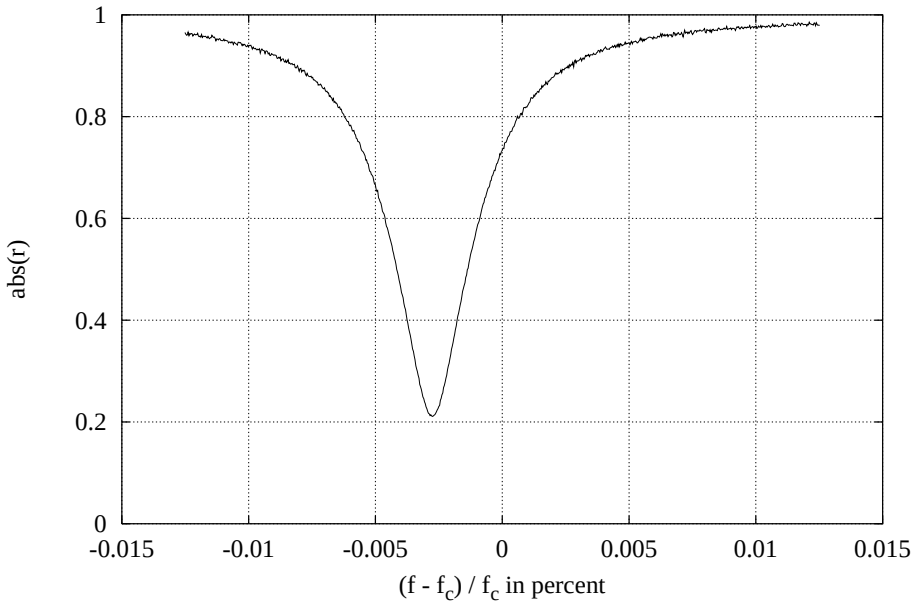

Figure 41: Input reflection corresponding to a single resonance as a function of frequency. Parameters: $f_c = 3.9965\,\mathrm{GHz}$, $N_f = 801$, $\Delta f_i = 3000\,\mathrm{Hz}$.

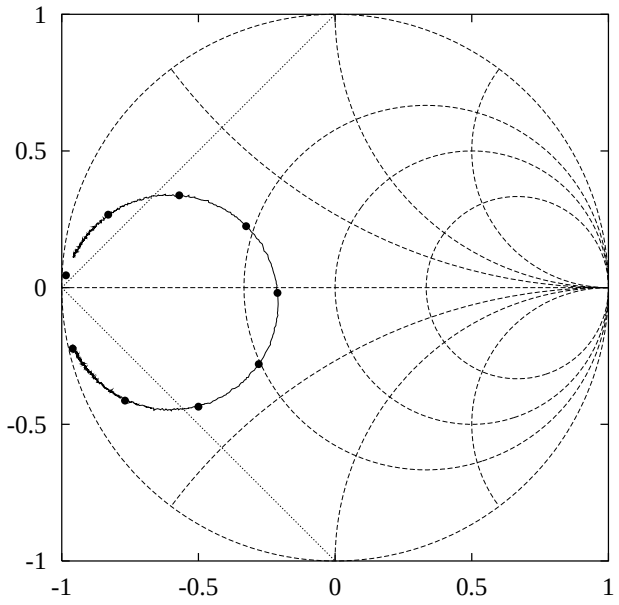

Figure 42: Smith chart corresponding to a single resonance. Parameters: see Fig. 41.

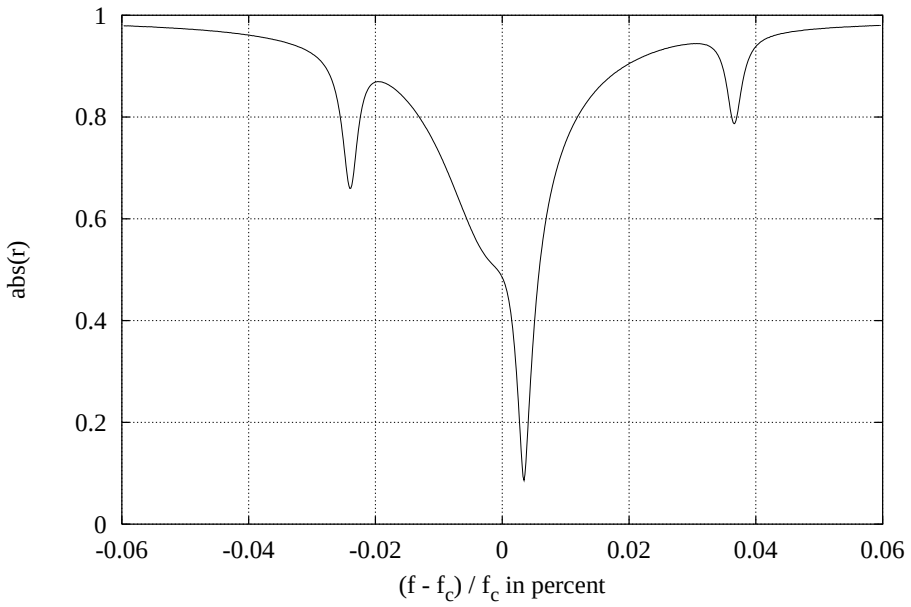

Figure 43: Input reflection corresponding to a triple resonance as a function of frequency. Parameters: $f_c = 3.35\,\mathrm{GHz}$, $N_f = 801$, $\Delta f_i = 30\,\mathrm{Hz}$.

Mode #	f_0 in GHz	Quality factor
1	3.349195	26000
2	3.350115	23000
3	3.351225	29000

Table 3: Resonant frequencies and quality factors of the modes corresponding to the measurement which is shown in Fig. 44.

is used by developed program in order to find R_{inf}. Our calculation yielded that the internal quality factor of this mode is about 31000.

The input reflection which is shown in Fig. 44 corresponds to three resonances which are close together. For this measurement, an intermediate frequency of only 30 Hz was used. This is the reason why the curve in Fig. 44 is almost free of any noise. Unfortunately each measurement including calibration of the VNA takes some minutes using such a small Δf_i.

Since the spectral distance between the resonances is so small, we expect that each of them is strongly affected by the other modes. The resonances should therefore not behave like single modes. This is confirmed by the corresponding Smith chart representation of Fig. 44. The input reflection curve consists basically of three loops each of them representing one resonance. These loops are quite different from the single mode circles which are used for the calculation of R_{inf}. This underlines the strong effect of parasitic modes on each resonance if the modes are not well-separated. The resonant frequencies and the quality factors of the three modes which correspond to the measurement that is shown in Fig. 44 are presented in Table 3.

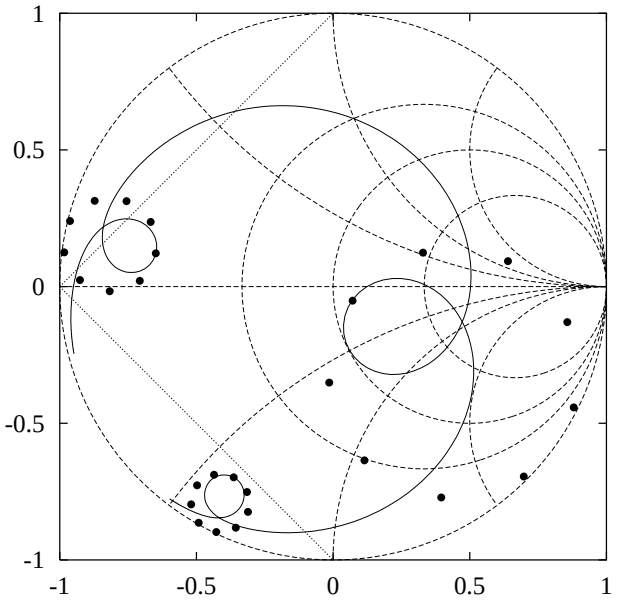

Figure 44: Smith chart corresponding to a triple resonance. Parameters: see Fig. 43.

IVc) Measurements with and without absorber

We already investigated the effect of a MACOR absorber on the quality factors of a superconducting TESLA 9cell structure in paragraph IIIc). On the other hand our measurements are based on a copper model. Hence the question arises whether the effect of the absorber can also be observed in such a conventional structure. Fig. 45 shows the calculated quality factors in the

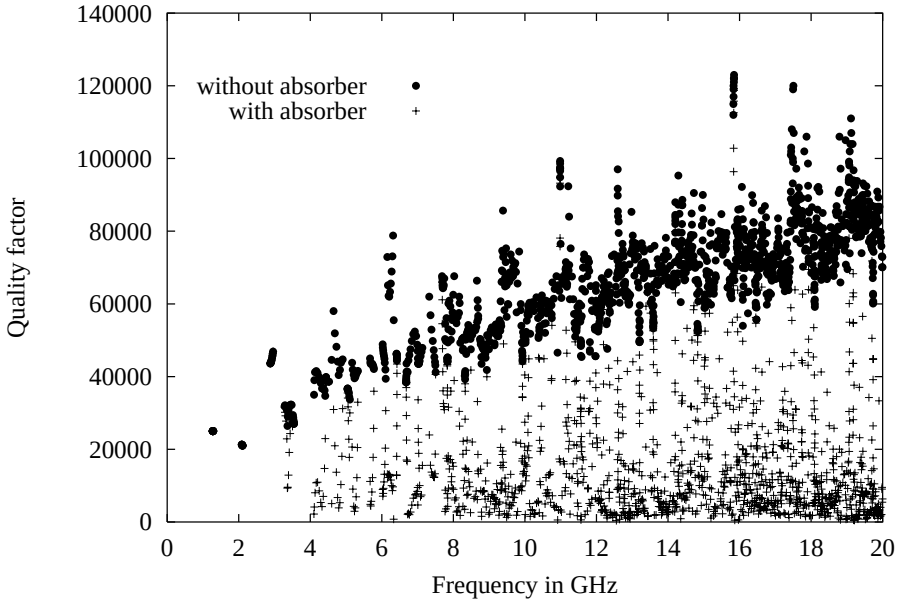

Figure 45: Calculated quality factors in the frequency range from 3 GHz to 20 GHz with and without absorber material. It is assumed that the absorber material has a thickness of 10 mm.

frequency range from 3 GHz to 20 GHz with and without absorber material. For the calculations it was assumed that the absorber material has a thickness of 10 mm. The fact that we use a copper structure instead of a niobium one is taken into account by setting the scaling factor α according to Eqs. (25) and (31) to unity. If we compare the results with and without absorber it can be concluded that we should clearly see the effect of the MACOR absorber even in the copper model at room temperature which means that the quality factors of the vast majority of modes are significantly reduced by the absorber.

In order to check the validity of our results let us consider a single passband with and without absorber material in more detail. The corresponding calculated results are presented in Fig. 46. If the absorber cavity is empty the quality factors are almost constant for all modes as expected.

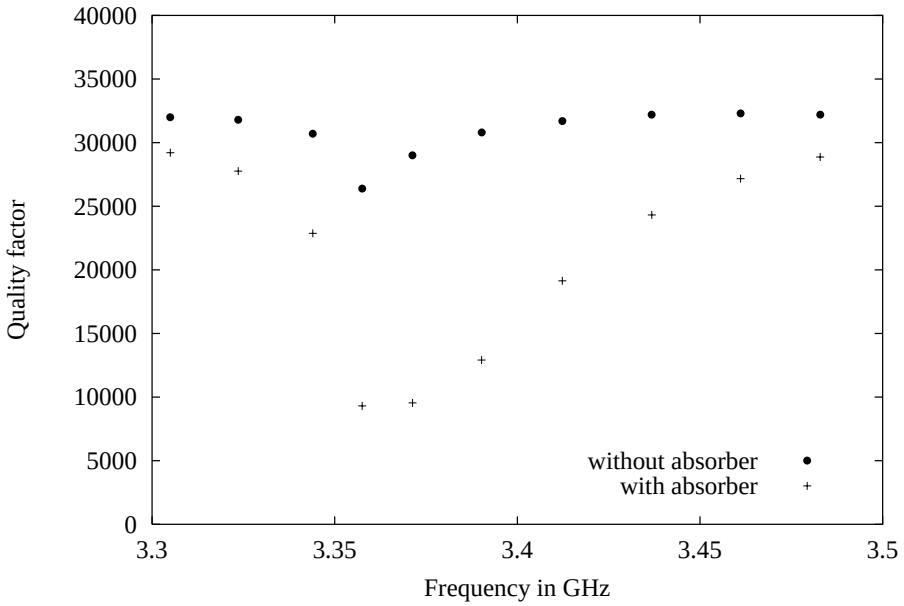

Figure 46: Calculated quality factors of a single passband with and without absorber material.

Those of the cavity modes with absorber material are always less than the corresponding values of the modes without absorber material. The reduction of the quality factors is however most efficient in the middle of the passband ($26000 \rightarrow 9000$); whereas the effect of the absorber is much weaker at its edges. This can be explained by a similar behaviour of the coupling of the modes of the 9cell structure to the beampipe [20]. Note that a shift of the resonance frequencies due to the real part of the permittivity of the absorber material is not included in our distortion analysis which only considers the losses. In Fig. 46 it is hence assumed that the modes with and without absorber material have the same resonant frequencies.

Fig. 47 shows the measured quality factors of a single passband. The results which are presented in this figure clearly show that the resonant frequencies of the modes with and without absorber material are not exactly identical. Apart from this fact the agreement between the values which are presented in Figs. 46 and 47 is quite well: Again each resonance with absorber material has higher losses than the corresponding resonance without absorber material; and the largest reduction of the quality factors is observed near the center of the passband ($29000 \rightarrow 6000$). The measured results thus confirm the validity of our analysis.

It would be desirable to check the performance of the MACOR absorber also at higher frequencies than 3.5 GHz. In principle, the current equipment which was described above allows

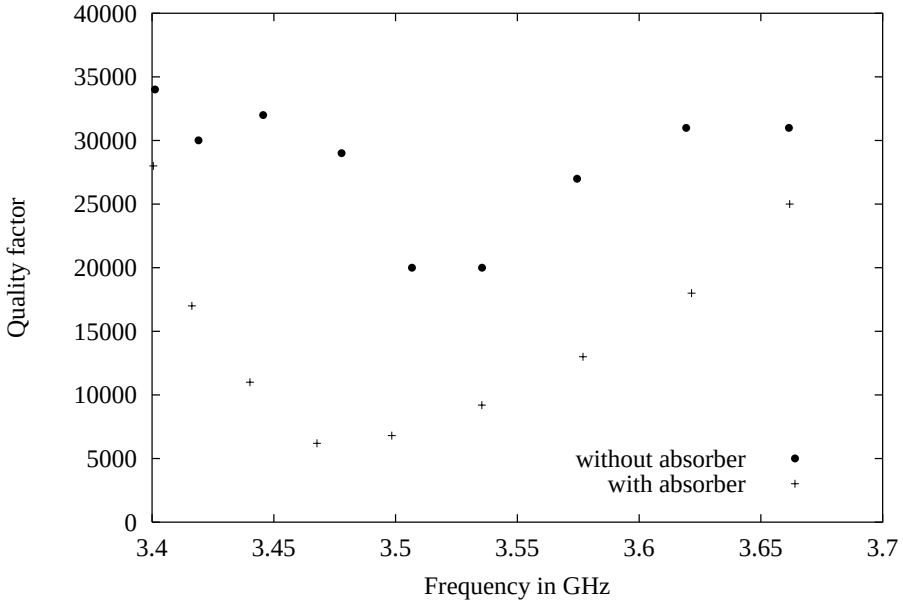

Figure 47: Measured quality factors of a single passband with and without absorber material.

measurements up to a frequency of 20 GHz. The number of resonant modes up to a certain frequency limit was estimated in paragraph IIa). There it was shown that the number of TM monopole modes of the investigated structure which have a resonant frequency less than 20 GHz amounts to about 1400. It is obvious that we cannot measure each of these modes. We thus concentrated on three frequency intervals: Fig. 48 shows the measured quality factors of about

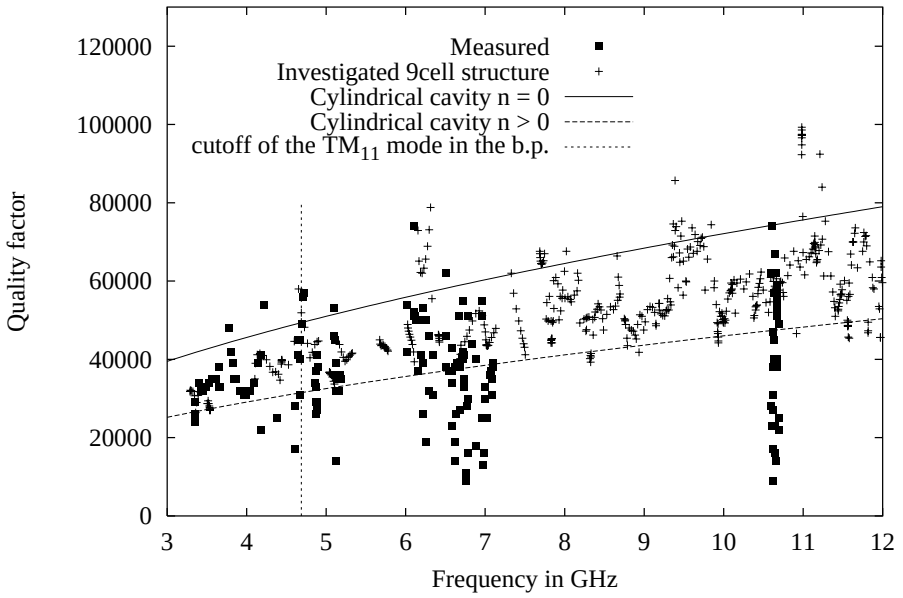

Figure 48: Measured quality factors of the copper model of the TESLA 9cell structure.

150 modes of the copper model of the TESLA 9cell cavity. Approximately 60 modes were found

in each of the two frequency ranges between 3.3 GHz and 5.2 GHz and between 6 GHz and 7.1 GHz. Between 10.6 GHz and 10.7 GHz another 30 modes were measured.

The results which are presented in Fig. 48 illustrate the difficulties that we encounter if we consider frequencies higher than 4 GHz. The values of the measured quality factors agree quite well with the theoretical predictions up to a frequency of about 4.5 GHz. On the other hand many modes with considerably lower quality factors than expected were found at higher frequencies which makes it almost impossible to recognize the effect of an absorber. To the authors opinion this might be explained by the excitation of higher order modes in the azimuthal direction due to small geometric imperfections. Since we did not measure the field distribution inside the investigated structure a number of resonances are probably dipole modes or modes with even a higher circumferential order instead of monopole modes that we are looking for. Note that the cutoff frequency of the TM_{11} mode in the beampipe is 4.7 GHz which is very close to the frequency where the deviations between theory and measurements are first observed. Furthermore the number of found modes in the frequency intervals at 7 GHz and 10 GHz is significantly higher than that which results from Eq. (11). This fact also confirms the suspicion of the authors that modes with higher circumferential orders are excited.

V Conclusions and outlook

In the field theoretical part of this contribution it was shown how the number of TM monopole modes in rotationally symmetric structures up to a certain frequency limit can be estimated. Moreover the simple model of a cylindrical cavity was used in order to study the losses of these modes as a function of the mode parameter. Then the GSM method was employed for the computation of the resonant frequencies, quality factors and loss parameters of a TESLA 9cell cavity which is connected to an absorber cell.

For the characterization of absorber materials a planar model was developed. As a reference material a very lossy glas, namely $0.5AgI{*}0.5AgPO_3$, was investigated. The conductivity of this material had already been measured at the Universität Münster up to a frequency of 10 THz. The effect of this material as a HOM absorber was studied by a distortion analysis based on the results of the GSM method. It turned out that almost all of the HOM energy can be absorbed by the suggested $0.5AgI{*}0.5AgPO_3$ absorber. Unfortunately this material cannot be used under vaccum conditions.

Alternatively MACOR was considered as absorber material. This ceramic is frequently used in the vacuum system of accelerators. The electromagnetic properties of MACOR at room temperature were known from the literature and from measurements at the Universität Hamburg and the Universität Münster. Based on the available data it was demonstrated that the performance of MACOR at 295 K as absorber material seems to be sufficient. Furthermore it was shown that the efficiency of the MACOR absorber at low frequencies can considerably be enhanced by increasing the thickness of the absorber cylinder.

The simulations also predict that the effect of the MACOR absorber should be observable in a copper structure. In order to confirm the results of the theoretical investigations, the quality factors corresponding to the resonances of a copper model of a TESLA 9cell cavity which was connected to an absorber cell were measured. Starting from a model for the input impedance for such a structure, a procedure was developed for the calculation of the internal quality factors of resonant modes from the input reflection which can be measured using a VNA. It was found that the measurements and the theoretical results agree quite well in the spectral range below the cutoff frequency of the TM_{11} waveguide mode. For higher frequencies more resonant modes

than expected were detected. The quality factors of the modes were in general less than the values which were predicted by the theoretical investigations for TM monopole modes. The authors suspect that these discrepancies between theory and measurements can be explained by parasiticly excited modes with a higher order azimthal dependence which still has to be checked by further measurements.

The simulation results for MACOR are based on material data which are valid at room temperature. On the other hand, the TESLA HOM absorber will be installed in a 70 K environment. It is expected that the material losses of MACOR at 70 K are significantly less than those at room temperature. An estimation of these losses based on an extrapolation of data for the far infrared regime yields that the performance of MACOR at 70 K as a HOM absorber will be acceptable if the HOM losses at the cold (2 K, 4 K) normal conducting elements of a module are not too high. But this has still to be investigated.

Acknowledgement

The authors are indebted to many colleagues from the TESLA collaboration who contributed to these ideas.

References

[1] R. Brinkmann *et al.* (ed.), *Conceptual design of a 500 GeV e^+e^- linear collider with integrated X-ray laser facility*, DESY 1997-048, 1997.

[2] R. Brinkmann, "On the free electron laser mode operation in TESLA", DESY, TESLA 96-01, 1996.

[3] A. Novokhatski, M. Timm and T. Weiland, "Single bunch energy spread in the TESLA cryomodule", DESY, TESLA 99-16, 1999.

[4] R. Brinkmann, M. Dohlus, D. Trines, A. Novokhatski, M. Timm, T. Weiland, P. Hülsmann, C. T. Rieck, K. Scharnberg and P. Schmüser, "Terahertz wakefields in the superconducting cavities of the TESLA-FEL linac", to be published.

[5] M. Dohlus, N. Holtkamp, A. Jöstingmeier, H. Hartwig and D. Trines, "Design of a HOM broadband absorber for TESLA", *Meeting note: 31 Linear collider project meeting at DESY*, 1998.

[6] M. Dohlus, N. Holtkamp and A. Jöstingmeier, "Design of a broadband absorber for $f >$ 100 GHz", *Meeting note: 26 Linear collider project meeting at DESY*, 1997.

[7] A. Jöstingmeier, M. Dohlus and N. Holtkamp, "Computation of the absorption characteristics of a two-dimensional rectangular waveguide array using the mode matching technique", DESY, TESLA 98-24, 1998.

[8] A. Jöstingmeier and M. Dohlus, "Comparison of the beam parameters corresponding to corrugated circular waveguides and planar gratings", DESY, TESLA 98-30, 1998.

[9] A. Jöstingmeier, M. Dohlus and N. Holtkamp, "Application of the mode matching technique for the computation of the beam parameters of an infinite periodic structure", DESY, TESLA 98-23, 1998.

[10] R. E. Collin, *Foundations for Microwave Engineering*, McGraw-Hill, 1966.

[11] J. M. Neilson *et al.*, "Determination of the resonant frequencies in a complex cavity using the scattering matrix formulation," *IEEE Trans. Microwave Theory Tech.*, vol. 37, pp. 1165–1169, 1989.

[12] T. Itoh, "Generalized scattering matrix technique," *Numerical Techniques for Microwave and Millimeter-Wave Passive Structures*, Wiley, New York, pp. 622–636, 1989.

[13] C. Rieckmann, A. Jöstingmeier and A. S. Omar, "Numerically efficient computation of a complete set of eigenfunctions in complex cavities," *Electromagnetics*, vol. 16, pp. 291–311, 1996.

[14] A. Jöstingmeier, M. Dohlus, C. Rieckmann and A. S. Omar, "Application of the GSM method and TD computation of the long range wake in linear accelerator structures," Proc. IEEE Particle Accelerator Conference (Vancouver), pp. 2553–2555, 1997.

[15] H. Matsumoto, *Private communication.*

[16] C. Cramer, K. A. I. El-Egili, J. Gockel, E. Grter-Hge, R. Holtwick, M. Lange, R. Pschel, D. Zurwellen and K. Funke, *Solid State Ionics*, to be published.

[17] K. Pathmanathan, S. R. Hope, G. P. Johari, *J. Non-Cryst. Solids*, vol. 94, 1987.

[18] M. N. Afsar and K. J. Button, "Millimeter-wave dielectric measurement of materials", Proc. IEEE, vol. 73, pp. 131–153, 1995.

[19] J. R. Birch, "Optical constants of some commercial microwave materials between 90 and 1200 GHz", Proc. IEE, vol. 130, pp. 327–330, 1983.

[20] M. Dohlus, *Private communication.*

Appendix

Let A^i and B^i denote the amplitudes of the incident and the reflected TEM wave in front of the absorber, see Fig. 16. The electromagnetic field in this region can then be written as

$$E_y^i = A^i e^{-jk_0 z} + B^i e^{jk_0 z} \quad , \tag{74}$$

$$H_x^i = \frac{1}{Z_0}\left(-A^i e^{-jk_0 z} + B^i e^{jk_0 z}\right) \quad , \tag{75}$$

where k_0 and Z_0 are the vacuum wavenumber and the intrinsic impedance of free-space. It is assumed that the incident TEM wave has a y- and a x-component of the electric and the magnetic field, respectively. The corresponding relations for the absorber field read

$$E_y^a = A^a e^{-jk_m z} + B^a e^{jk_m z} \quad , \tag{76}$$

$$H_x^a = \frac{1}{Z_m}\left(-A^a e^{-jk_m z} + B^a e^{jk_m z}\right) \quad . \tag{77}$$

In the above equations k_m and Z_m denote the wavenumber and the intrinsic impedance of the absorber material:

$$k_m = \sqrt{\varepsilon_r' - j\varepsilon_r''}k_0 \quad , \tag{78}$$

$$Z_m = \frac{Z_0}{\sqrt{\varepsilon_r' - j\varepsilon_r''}} \tag{79}$$

ε_r' and ε_r'' are the real and the imaginary part of the relative permittivity of the absorber. Note that k_m and Z_m are complex-valued numbers in contrast to k_0 and Z_0. The region behind the absorber is assumed to be matched. Therefore only an outgoing wave exits for $z > d$:

$$E_y^t = A^t e^{-jk_0(z-d)} \quad , \tag{80}$$

$$H_x^t = -\frac{A^t}{Z_0} e^{-jk_0(z-d)} \tag{81}$$

The field expansion coefficients B^i, A^a, B^a and A^t can be straightforwardly calculated as a function of the amplitude of the incident field A^i by making use of the well-known continuity conditions of the electromagnetic field at the two interfaces at $z = 0$ and $z = d$:

$$B^i = A^i \frac{Z_m - Z_0}{Z_m + Z_0} \frac{1 - e^{-j2k_m d}}{1 - \left(\frac{Z_m - Z_0}{Z_m + Z_0}\right)^2 e^{-j2k_m d}} \quad , \tag{82}$$

$$A^a = A^i \frac{2Z_m}{Z_m + Z_0} \frac{1}{1 - \left(\frac{Z_m - Z_0}{Z_m + Z_0}\right)^2 e^{-j2k_m d}} \quad , \tag{83}$$

$$B^a = A^a \frac{Z_0 - Z_m}{Z_m + Z_0} e^{-j2k_m d} \quad , \tag{84}$$

$$A^t = A^a \frac{2Z_0}{Z_m + Z_0} e^{-j2k_m d} \tag{85}$$

The absorber losses are given by

$$P_{loss} = \omega \int_{z=0}^{d} \frac{\varepsilon''}{2} \left|E_y^a\right|^2 dz \quad . \tag{86}$$

In order to evaluate the above equation we use the representation according to Eq. (76) for the electric field E_y^a which yields

$$P_{loss} = \frac{\varepsilon_r'' k_0 d}{4Z_0} \left(|A^a|^2 \frac{e^{2\mathrm{Im}\{k_m\}d} - 1}{\mathrm{Im}\{k_m\}\, d} - |B^a|^2 \frac{e^{-2\mathrm{Im}\{k_m\}d} - 1}{\mathrm{Im}\{k_m\}\, d} - 2\mathrm{Re}\left\{ A^a B^{a*} \frac{e^{-2j\mathrm{Re}\{k_m\}d} - 1}{j\mathrm{Re}\{k_m\}\, d} \right\} \right) . \tag{87}$$

The absorber losses may also be calculated from the law of power conservation:

$$P_{loss} = \frac{1}{2Z_0} \left(\left|A^i\right|^2 - \left(\left|B^i\right|^2 + \left|A^t\right|^2 \right) \right) \tag{88}$$

P_{loss} is always computed from Eqs. (87) and (88) in order to check the analysis.